RADIATION DAMAGE AND COLOR CENTERS IN ZnF_2 AND MgF_2

By

CHARLES THOMAS BUTLER

Bachelor of Science
Iowa State University
Ames, Iowa
1954

Master of Science
Texas A & M University
College Station, Texas
1957

Submitted to the Faculty of the Graduate College
of the Oklahoma State University
in partial fulfillment of the requirements
for the Degree of
DOCTOR OF PHILOSOPHY
July, 1972

RADIATION DAMAGE AND COLOR CENTERS IN ZnF_2 AND MgF_2

Thesis Approved:

W. A. Sibley
Thesis Adviser

J. Paul Denham

James N. Lange

E. E. Taylor

D. Durham
Dean of the Graduate College

TO

Joye, my Mate

Beth, my Princess

Debbi, my Jewel

David, my Son

ACKNOWLEDGEMENTS

Throughout this research, W. A. Sibley has shown himself first the friend which he has been for some time, and second a steady guide and counsellor in the technical areas covered.

E. Sonder of the Oak Ridge National Laboratory was very helpful during the radiation damage studies. I am grateful to F. A. Sherrill of that institution for orienting some of the crystals used, and to the Solid State Division of that Laboratory for use of their electron Van de Graaff accelerator. Of the many persons at this University who have been of help, the author wishes to express his special gratitude to H. Hall and S. I. Yun for their assistance during this work.

To Joye, my wife, I express my deepest appreciation for her encouragement and for her assistance in preparation of this dissertation.

TABLE OF CONTENTS

LIST OF TABLES

LIST OF FIGURES

LIST OF FIGURES (Continued)

CHAPTER I

INTRODUCTION

The study of defects occupies a prominent position in our efforts to understand the solid state. From defect studies has come an increased understanding of the perfect lattice as well as many of the technological advances of recent years. Insulating crystals, and in particular polar insulators, are often chosen for defect studies. Because they are optically transparent over a wide range of wavelengths, they can be investigated by means of their optical absorption and emission in addition to the mechanical, electrical and thermal techniques employable with optically opaque solids.

Broadly speaking, defects in solids can be characterized as being either of point or extended nature[1]. Dislocations, grain boundaries, and macroscopic inclusions fall into the latter category, while point defects--the ones of interest in this work--include single or small groups of lattice vacancies, interstitials, or impurities. The study of impurity centers comprises a large and important field of investigation; however, this present work is restricted to the study of certain non-impurity point defects. Such defects are termed color centers, the name given them by early workers, because their presence often causes the normally transparent host crystal to become deeply colored. Indeed, it is just this coloration which makes study of these defects in transparent crystals experimentally attractive.

Color centers may be created in a crystal by mechanical deformation[2]. In this production process, many extended defects are also formed, making study of isolated color centers difficult or impossible; therefore, this method of introduction is seldom used. A second technique, more often used than the former, consists of heating the host crystal in the presence of the vapor of one of its constituent elements --usually the cation or positive ion[3,4]. This technique, called additive coloration, is restricted to introduction of only the simplest centers, but is often valuable for just this reason. One need not contend with interference from more complex centers while making measurements. In the third and most common coloration method, the crystal is irradiated with energetic particles or photons. Although many types of point defects are formed by such treatment, most of them can be studied without undue interference from the others. Moreover, there are many lattice defects which can be controllably introduced only by irradiation. The centers studied in this work were introduced into the lattice by bombardment with 2.0 MeV electrons from a Van de Graaff accelerator at the Oak Ridge National Laboratory.

When an energetic photon or particle strikes a polar crystal, it can cause lattice damage in two distinct ways. First, it can displace lattice atoms by an elastic or billiard-ball collision. The efficiency of this so-called knock-on process, of course, is dependent upon the energy of the bombarding particle, but is also highly anisotropic because of the existence of channeling and focusing directions in the crystal lattice[5-8]. In these directions, damage may be easily created, while in others, the lattice may be highly resistant to damage.

Knock-on damage is produced in all materials. The second type of

damage, termed radiolysis, is confined exclusively to insulators. It is photochemical in nature, and can result if the incident particle, or a secondary resulting from a knock-on collision is charged, or if high-energy photons are employed. The exact mechanism of this process is not yet fully understood, but of the various suggestions in the literature[9,10], that with the widest acceptance is due to Hersch[11,12] and Pooley[13]. In their mechanism for photochemical damage, an electron is removed from a lattice ion in an ionization event, leaving a hole behind. The lattice ions quickly adjust their positions to reflect the new local potential. This leads to a configuration in which the hole is self-trapped on two adjacent anions which have moved together slightly. The energy relative to the lattice of this center can be considerable--about the width of the bandgap[14]. When the self-trapped hole and an electron recombine, that part of the energy due to polarization of the lattice is suddenly released, allowing one of the two anions involved to recoil with enough momentum to remove it from its lattice site to an interstitial position. The resulting damage centers are an interstitial and an anion vacancy containing an electron. These are stable if the interstitial is trapped by an interstitial cluster, impurity or some extended defect, or if the temperature is too low for the interstitial to diffuse back to its vacancy. One mechanism which greatly enhances the probability that the interstitial will end up far from its vacancy and thus be trapped before it can recombine with its vacancy is the replacement collision sequence or focusing collision already mentioned in connection with the knock-on process. If focusing directions exist in which the recoiling anion is likely to move, the interstitial may indeed be produced many lattice spaces from its vacancy. In the past, some have

deemed such replacement sequences to be essential to the Pooley-Hersch damage mechanism[11-14]. Magnesium Fluoride and ZnF_2 are of the rutile structure (tetragonal) for which no obvious focusing directions exist. Yet, MgF_2 damages photochemically[15-17]. One of the goals of this work was investigation of the damage mechanism of ZnF_2 in order to further assess the importance of focusing collisions in the photochemical coloration process.

In principle, the simplest damage centers could consist of vacancies on the anion and cation sublattices, anion or cation interstitial atoms or ions, and electrons or holes self-trapped or trapped at impurities or extended defects[1]. Nearly all of these have been found, but by far the most common and most extensively studied defects in polar crystals are the F-type centers which consist of single anion vacancies which have trapped one or more electrons. Aggregates of F centers are not uncommon and are designated F_2, F_3, ... centers, depending upon the number of aggregated vacancies involved[18]. Reference 10 lists the most common defect types and suggests a uniform system of notation. This system has been used throughout this work. The principal damage centers created in ZnF_2 under the treatments given it here were the F and F_2 which are a single anion vacancy containing a single electron, and two adjacent F centers, respectively. In addition, a center tentatively identified as the $[F_2^-]$ has been observed during low temperature irradiations. This $[F_2^-]$ center, which is a hole self trapped on two adjacent anions, should not be confused with the di-F or F_2 center. Figure 1 depicts the ZnF_2 lattice. There are two orientationally non-equivalent F centers in the rutile-structure lattice, each with C_{2v} site symmetry. These two types of F centers, labeled A and B in the figure, should be energetically

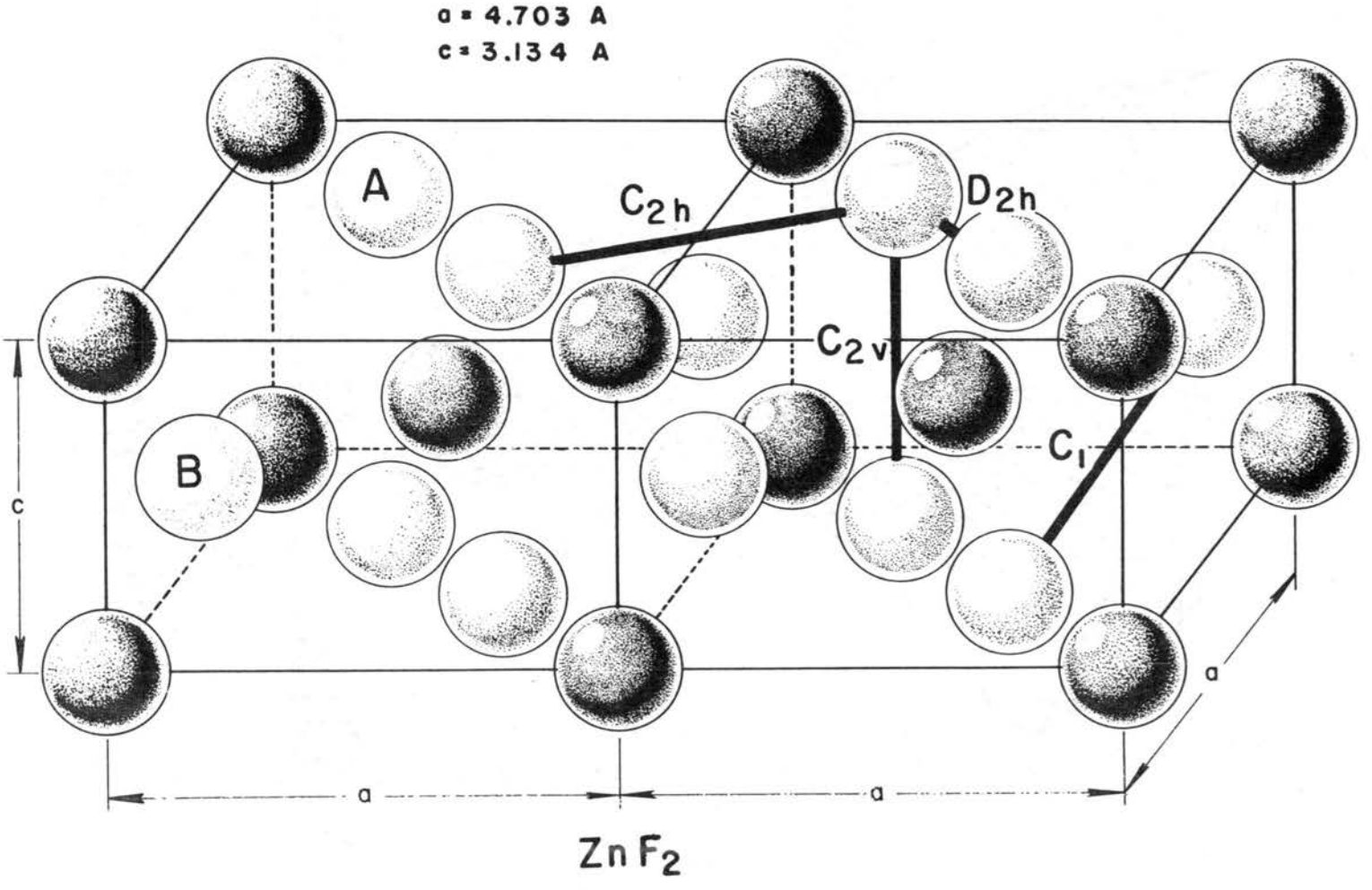

Figure 1. The ZnF_2 Lattice, Showing the Sites of the Two F and the Four Possible F_2 Centers

equivalent. There are four possible F_2 centers, also indicated in the figure and labeled according to their site symmetries.

To investigate these centers, the techniques of polarized optical absorption and emission were employed. Optical absorption of an F or F_2 center arises from excitation of one of its trapped electrons. If the center posesses a unique orientation in the lattice, such as the C_{2h} F_2 center of Figure 1, the optical transition moments reflect this symmetry. A correlation of the anisotropy expected for a given center with that actually found for the various optical absorption bands furnishes strong evidence of the identification of the color center responsible for those bands. The F band in this material has been tentatively identified on the basis of its absorption energy, and the fact that the F band in most materials is the most prominent band in the absorption spectrum after prolonged irradiation.

In summary, then, the broad aims of this work were threefold: to tentatively identify the principal damage centers produced in nominally pure ZnF_2 by 2 MeV electrons, to suggest the damage mechanisms operative in this material by investigation of the type and rate of color center formation as a function of temperature, and to investigate in some detail the changes of the peak position and half width of the C_{2h} F_2 center with temperature so that some idea of the interaction of lattice modes with defects could be obtained.

CHAPTER II

CRYSTAL GROWTH AND CHARACTERIZATION

Apparatus

The ZnF_2 crystals required for this work were grown by a modification of a method originally introduced by Bridgman[19] and Stockbarger[20,21]. In this method, a melt contained in a suitable crucible is slowly lowered from a region in which the temperature is above the melting point into one in which the temperature is below the melting point. Such a system is shown schematically in Figure 2. It is apparent that raising the furnace around the crucible would be essentially equivalent to lowering the crucible through the furnace. Because the crucible is often contained in an immobile vacuum system, raising the furnace is not uncommon.

In a Bridgman apparatus, the most important single parameter is the shape and magnitude of the temperature gradient through which the crucible is moved. Ideally, this gradient should be infinite. In practice, values from 20 to 50°C/cm are usually found. If the gradient is too small, several deleterious effects result. First, bulk nucleation may occur ahead of the growth interface. Because their solubilities are less in the solidous than in the liquidous phase, impurities are concentrated in the region just ahead of the growth area. Such a situation, known as constitutional supercooling, leads typically to some form of cellular growth in which the impurities are concentrated in thin, mem-

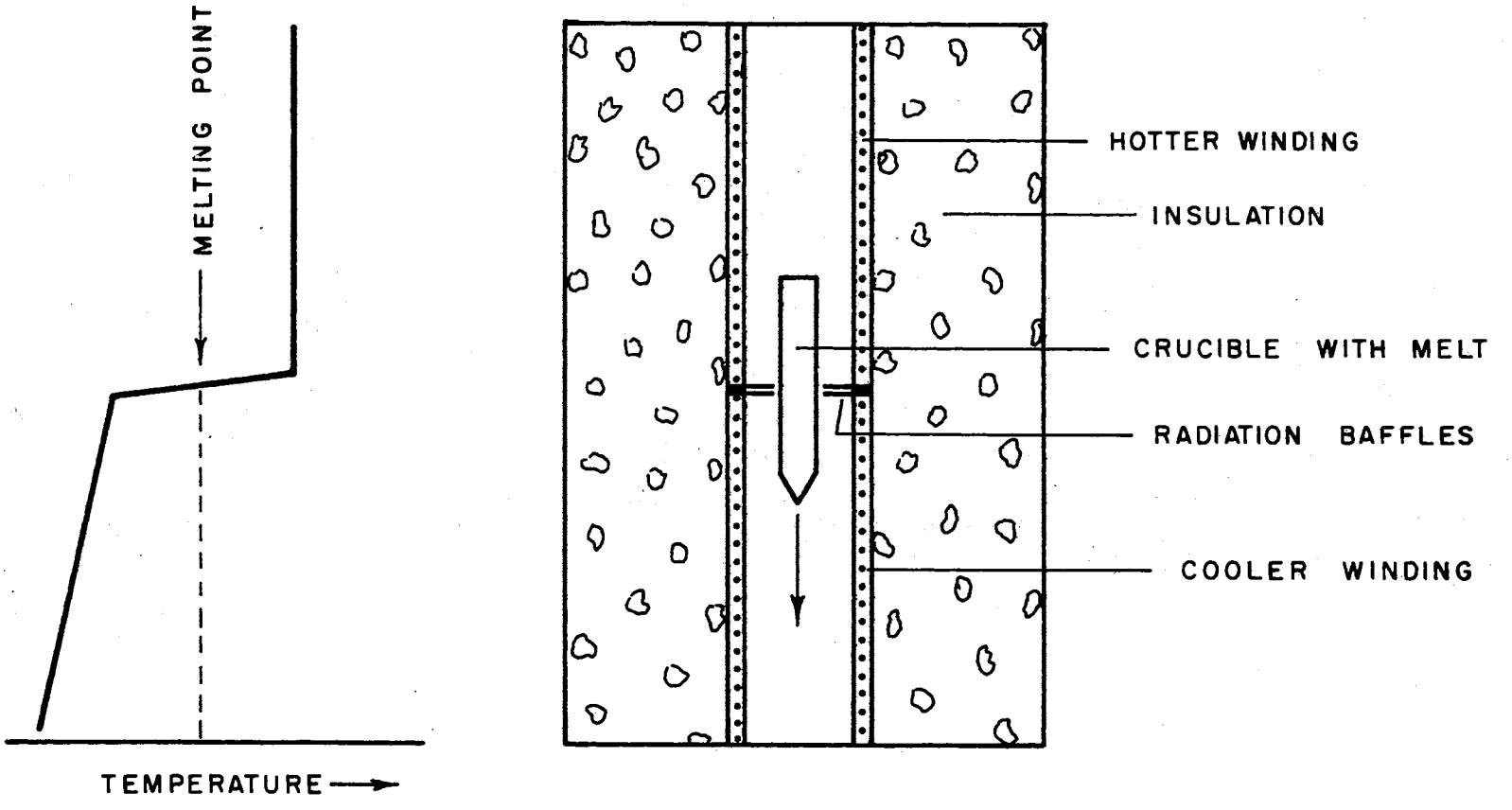

Figure 2. Schematic Bridgman Apparatus With Idealized Temperature Profile

brane-like structures which separate axial columns of normal crystal [22-24]. In such a case, polycrystalline or badly deformed crystalline material results. A second unwanted effect which results from too small a gradient is dendritic growth[22-24]. Release of the heat of solidification can cause a region to exist in the liquid in which the temperature is lower than that at the interface. Under these conditions, tree-like extensions may be nucleated ahead of the interface. This so-called dendritic growth results almost invariably in a polycrystal. Both of these effects may be mollified to some extent by moving the gradient through the crucible at a slow rate. Because of this, growth periods of many days or even weeks are not uncommon with the Bridgman method. Nevertheless, it remains one of the most important growth techniques because of the large spectrum of materials which can be grown using it--materials which often are difficult or impossible to grow by any other method.

The apparatus used in this work, shown in Figure 3, was designed to provide an adequate temperature gradient while allowing convenient handling of the reactive, toxic fluorides being grown. The crucible containing the melt is held in a graphite heat sink at the bottom of a ceramic vacuum tube. A small furnace is raised around this tube to move the temperature gradient through the crucible. Platinum windings are used to provide long furnace life at the high temperatures required for growth of the higher-melting fluorides. A fixed outer shell containing only insulating materials surrounds this heated, movable core to reduce heat losses. In this apparatus, the temperature gradient at the growing interface is increased over that which would exist naturally by two means. First, two annular radiation baffles are placed at the lower

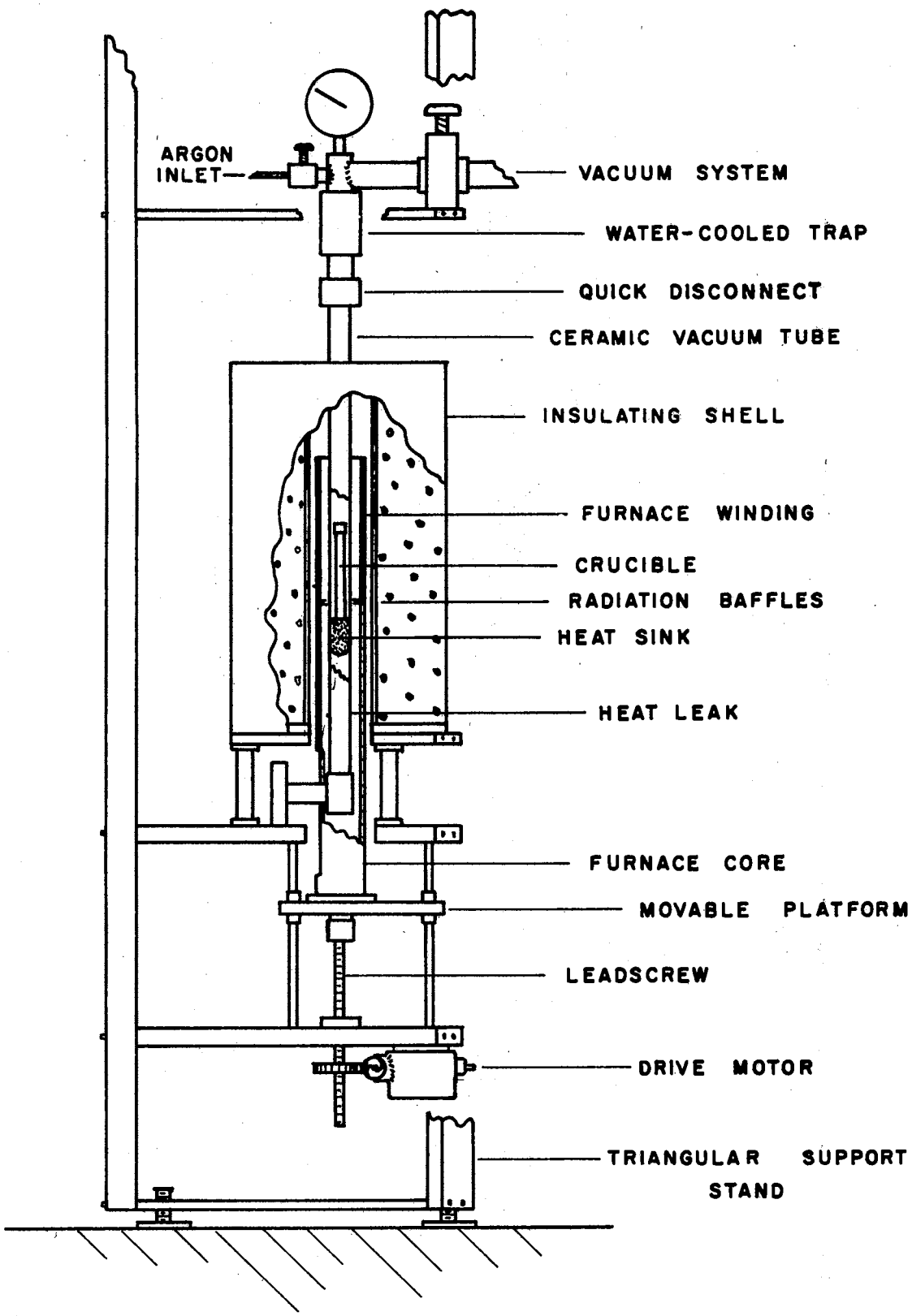

Figure 3. The OSU Bridgman Apparatus

edge of the Pt furnace windings. Second, a ceramic tube is brought into contact with the vacuum tube to help conduct away the heat of solidification as it is released. These two devices also help produce the proper shape for the growth interface by causing a melting isotherm convex into the liquid. If the heat of solidification were merely allowed to radiate from the crucible in the vicinity of the interface, a melting isotherm concave toward the liquid would result. At best, an interface of this shape tends to produce badly strained crystals, because any dislocations or other imperfections created at the rough crucible wall are incorporated into the crystal as it grows. At worst, the boule may become polycrystalline from propagation of microcrystals nucleated at the wall. A melting isotherm convex into the liquid tends to exclude these imperfections as the interface moves through the length of the crucible. The double expedient of removing the heat of solidification downward away from the interface, and of making the crucible from a material having a higher thermal conductivity than the crystal produces the desired convex growth interface.

Figure 4 presents temperature profiles along the crucible for this apparatus for two positions of the furnace relative to the crucible. The setpoint of the furnace windings was arbitrarily chosen as 1025°C for the measurements shown. Determination of the profiles was accomplished by sliding a movable thermocouple along the wall of an empty crucible while the furnace was operating under otherwise normal conditions. The approximate position of the crucible is shown in the figure. This setpoint is apparently appropriate for a material having a melting point of 800-850°C. It can be seen that the temperature gradient at the growth interface is near 30°C/cm. For setpoints near 800°C, this value

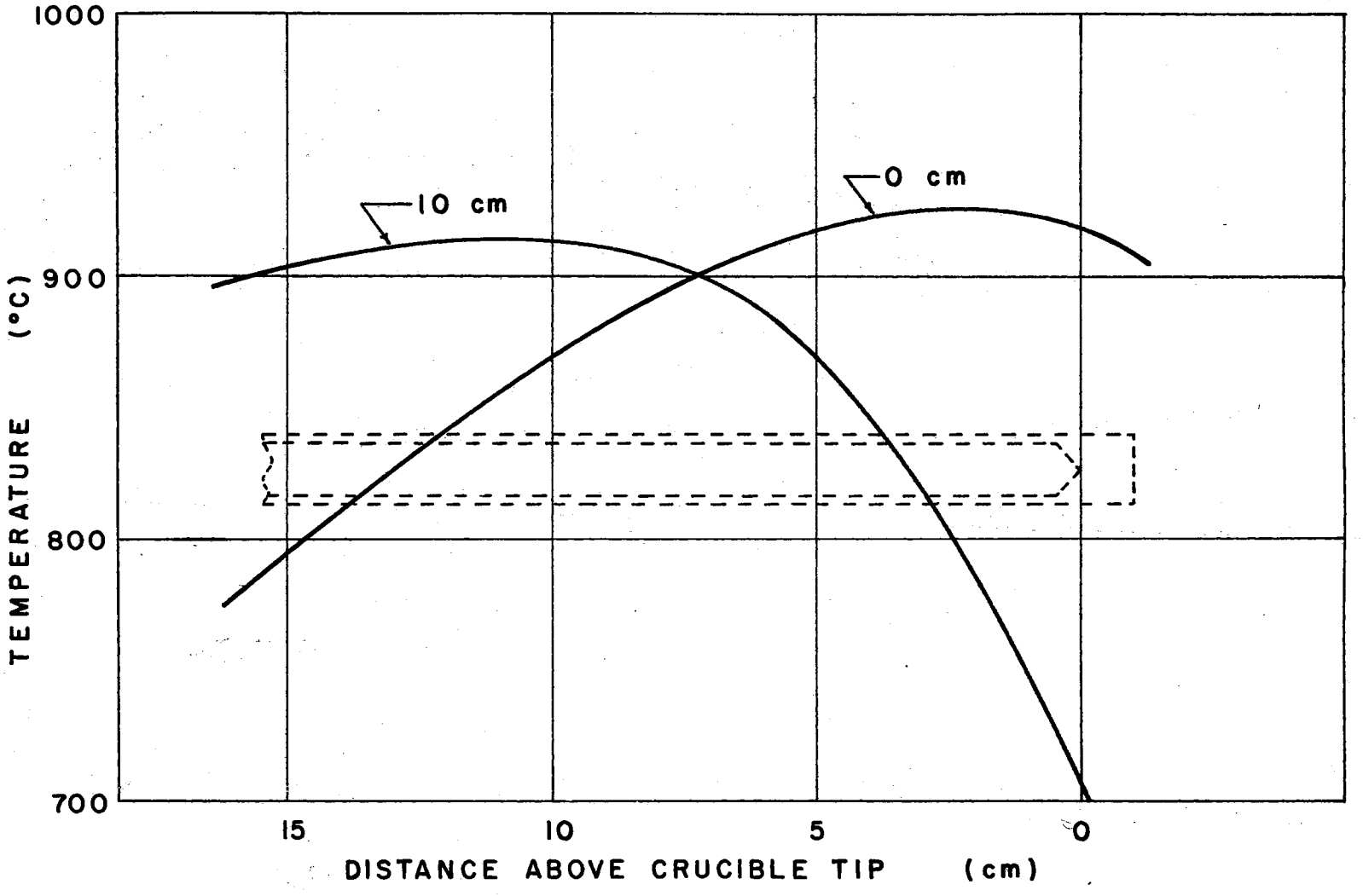

Figure 4. Measured Temperature Profiles in Bridgman Apparatus

falls to nearer 20°C/cm, and is appropriately higher for higher set-points.

Figure 5 shows details of the platinum-wound furnace. It is wound on a Norton high-purity alumina core from approximately 12 m of 0.810 mm (0.0319") diameter Pt wire. Region A on the figure is wound at 2.36 turns per cm (6 turns per inch), region B at half and region C at one-third this value. This winding pattern results in a nearly uniform temperature profile for the windings themselves. The remainder of the figure is self explanatory.

The vacuum system for the apparatus consists of a T-M Vacuum Products 200 l/s diffusion pump backed by a Welch 3 l/s forepump. This system is capable of reducing the pressure in the tube to 10^{-6} Torr in less than five minutes from a cold start. A bourdon gauge calibrated from -1 to +2 atmospheres (gauge) serves to monitor the Ar pressure in the system. The ceramic vacuum tubes are of Coors Mullite and are nominally 3.8 cm in outside diameter, 3.2 cm in inside diameter, and 76 cm long. One end is rounded and closed. These tubes are selected by the supplier to be within ±0.66 mm of the nominal outside diameter over the top 5 cm. The raising mechanism has a maximum travel of 23 cm and can move the inner furnace at speeds of nominally 1.5, 0.76, 0.30, 0.15, 0.08, or 0.03 cm/hr. A limit switch can be set to stop the travel at any desired point. It also can initiate an automatic temperature reduction program on the commercial temperature controller. This controller, purchased from Bruce Industrial Controls, Inc., comprises a standard three-action closed-loop system with a silicon controlled rectifier power stage.

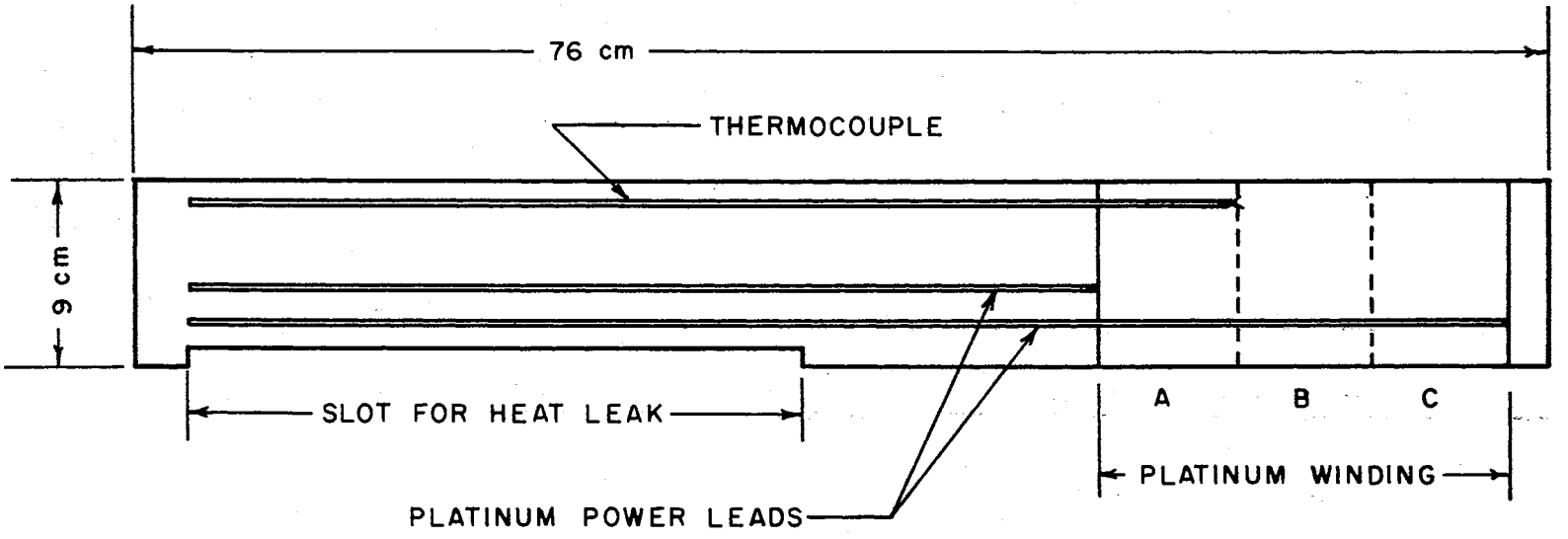

Figure 5. Details of the Platinum-Wound Furnace

Growth Procedure

Approximately 35 g of high purity, anhydrous ZnF_2 powder is placed in a high-purity graphite crucible in a controlled atmosphere glove box containing purified Ar gas. The crucible is fabricated from Ultra Carbon Corporation grade UT-9 graphite, and is shown in Figure 6. If there is reason to believe that the ZnF_2 may contain sorbed water, a 1 mm^3 piece of anhydrous ammonium bifluoride is put in the crucible first. This compound decomposes near 200°C, releasing HF gas which acts as a desiccant for the ZnF_2 powder. A screw cap containing a small axial hole is placed on the crucible, and the assembly, in its heat sink, is inserted into the ceramic tube. If a vent hole is not provided in the cap, the molten ZnF_2 is forced through the porous graphite crucible by its own vapor pressure. This tube is inserted into the furnace, connected to the vacuum system by means of a quick disconnect, axially aligned, and pumped to as low a pressure as possible. The high vapor pressure of the ZnF_2 prevents the pressure from falling below about 1 mtorr. (One millitorr is equal to a pressure of 1 micron of Hg.)

The Pt furnace, at its lowest position, is brought to its operating temperature over a period of several hours. Before the crucible has reached about 500°C, the vacuum tube is alternately filled with Ar and evacuated several times to displace unwanted gases. After the final evacuation, it is left filled with Ar at a gauge pressure of 500 torr. When the furnace has stabilized at its operating point, the raising motor is started. At the 3 mm/hr raising speed used for ZnF_2, 3-4 days are required to complete this phase of the growth process. When the furnace has reached its upper limit of travel, the limit switch stops the motor and starts an automatic program which lowers the temperature

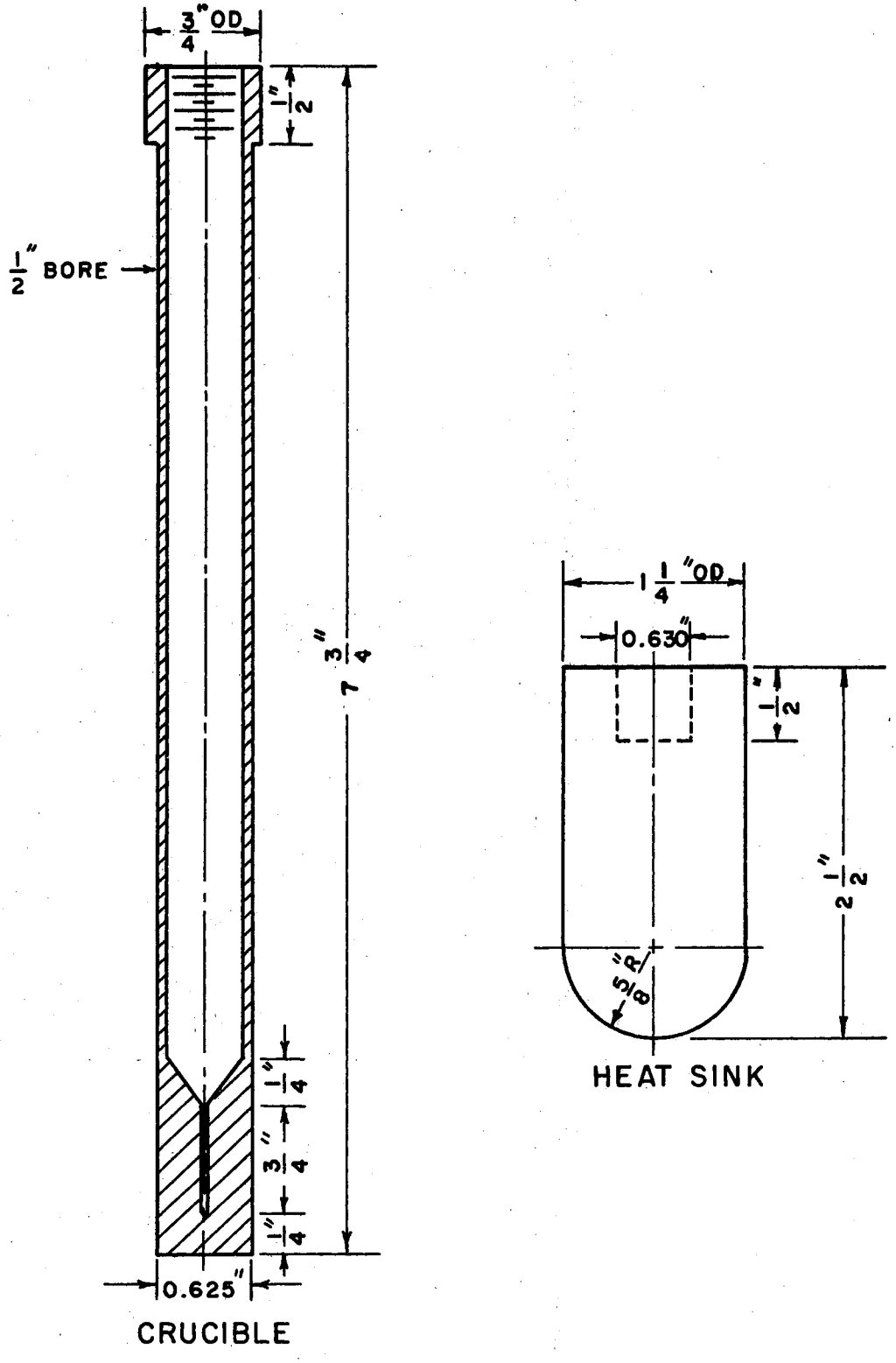

Figure 6. Graphite Crucible Design Used With the Apparatus

of the furnace to ambient over a 24-36 hour period. If the furnace is merely shut off, the crystal, ceramic tube or crucible sometimes crack from thermal shock. After the system has completely cooled, the tube is evacuated to vent free F_2 gas from the system, back filled with Ar, and removed. The crucible is then taken from the tube. Although ZnF_2 does not wet graphite, the boule often will not slide out of the crucible because of irregularities in the wall. If this occurs, the crucible is carefully sawed open to remove the crystal. Each crystal is assigned a serial number consisting of the date growth was begun: for instance, crystal 081971 was started on August 19, 1971.

A typical boule has a mass of 20-25 g and is single over the bottom 3-4 cm: the upper 2-3 cm are invariably polycrystalline. There are several possible explanations for this behavior. It may be that the heat of solidification cannot be removed rapidly enough by conduction down the crystal after it reaches a certain length. The maximum rate at which the crystal interface could grow would decrease with time in such a case, and would eventually fall below the rate at which the gradient were being moved. A second possibility is that the thermal convection pattern in the melt causes large enough temperature fluxuations at certain critical lengths of the liquid column to permit the growth rate of the interface to exceed, for a short time, the maximum permissible value[25-28]. A third possibility is suggested strongly by two observations: First, free F_2 gas exists in the vacuum system after each run, and tiny hexagonally-shaped metal crystals are found on the outside of the ceramic vacuum tube at the level of the crucible when the system is dismounted after a run. Second, the hexagonal cellular growth pattern characteristic of constitutional supercooling is observed in about the

last cm of each boule. These two facts indicate that ZnF_2 decomposes significantly at or just above its melting point. The metal crystals found on the ceramic tube are assumed to be Zn, since it is the only metal present in the system which crystallizes in a hexagonal habit. Excess Zn would, of course, be present in the melt, and would initiate constitutional supercooling at the level of the boule at which its concentration reached the critical value. It is this decomposition, with concurrent evaporation, which precludes lowering the growth rate to counteract the first and third possibilities above. As it is, approximately 20% of the mass of the charge is lost from the crucible during a run. Growing at the next slower rate would leave just about the amount of material in the crucible which is now obtained as single crystal. Nothing, therefore, would be gained.

Characterization

For investigations into such things as the detailed process of color-center stabilization or aggregation kinetics, a knowledge of the concentrations of all major impurities is essential. However, this present work is concerned simply with identification of the major color centers and the general mode of radiation damage in ZnF_2. Neither of these require a detailed knowledge of the impurities present. The impurities listed by BDH, Ltd., for their Optran grade ZnF_2 powder--the starting material used for these crystals--include Cd and Si at concentrations of 10-100 μg impurity per g ZnF_2 (μg/g), Cu and Fe at the 1-10 μg/g level, and As, Be, Ca and Mg below 1 μg/g. Typically, the expected concentration of an impurity in a crystal is about one tenth the concentration of that impurity in the starting material. Studies using the

technique of electron paramagnetic resonance indicate the presence in the crystals of Mn at a level near 10 μg/g, and of perhaps Cr and V at concentrations nearer 1 μg/g.

Zinc Fluoride does not normally cleave; however, it was found that a boule could be thermally fractured along a crystallographic plane by placing it on a hotplate. Laue photographs taken here, and others taken by Mr. Frank Sherrill of the Oak Ridge National Laboratory, verified that these planes were of (110) type with the [001] direction (the c axis) in the plane of the fracture. This method of finding the major crystallographic planes of the crystals proved invaluable, since it normally requires great labor to orient a boule for which no natural cleavage plane exists. Fortuitously, these natural fracture planes were the very ones needed for those parts of this work involving optically anisotropic centers.

Optical specimens were cut parallel to the thermal fracture planes using an Imanco Macrotome diamond saw, and polished using a Syntron LP-01 vibratory polisher with a Linde A/distilled water slurry. Any major irregularities were removed before polishing by hand lapping on a glass plate with number 600 carborundum grit in mineral oil.

CHAPTER III

THE THEORY OF OPTICAL TRANSITIONS IN COLOR CENTERS

The Absorption Position of the F Center

The very nature of the F center--an electron stably trapped at a lattice vacancy--suggests that a qualitative understanding of its general optical properties could be gained by considering a simple model: a particle in a three-dimensional infinite square-well potential.

The eigenstates for this model are well known[29] and are given by

$$E_n = \frac{\hbar^2 \pi^2}{2m}\left[\frac{n_1^2}{a^2} + \frac{n_2^2}{b^2} + \frac{n_3^2}{c^2}\right],$$

where m is the mass of the electron, n_1, n_2, and n_3 are the quantum numbers associated with each degree of freedom, and a, b, and c are the dimensions of the well. For a cubic well, a = b = c, and for a transition from the ground state ($n_1 = n_2 = n_3 = 1$) to the first excited state ($n_1 = n_2 = 1$; $n_3 = 2$), it is easily seen that

$$\Delta E = \frac{3\hbar^2 \pi^2}{2 m a^2} \tag{3.1}$$

The F absorption band is just such a transition, and we should expect this transition energy, ΔE_F, to follow a relation $\Delta E_F = Aa^{-2}$. This result was first noted by Mollwo[30] and later was modified by Ivey[31]. For the F center in alkali halides, the relation is found to be $\Delta E_F =$

$17.7a^{-1.84}$, where a is the nearest-neighbor distance for the vacancy. It can be seen that if a were to take on a range of values about some equilibrium value, that transitions would occur for a range of values about ΔE_F. In crystals at finite temperature, then, even this simple model predicts finite bandwidths due to ionic thermal vibrations.

In the rutile structure, there are two energetically equivalent types of F centers, labeled A and B in Figure 1, each with C_{2v} site symmetry. For this symmetry group, the three coordinate axes of the center all belong to separate representations. In our model, this corresponds to the situation $a \neq b \neq c$. We expect, then, three separate F transitions in ZnF_2. The energy differences between these transitions could easily be too small to be resolved in the real case, however, because of the thermal broadening just mentioned. We shall discuss widths of optical transitions at finite temperatures in more detail later. In this section, however, only the transition energies at zero K will be considered.

There have been many attempts to use more realistic models to predict the absorption energy of the F center at zero K[29]. The two models we shall consider are the point-ion and the extended-ion approximations. The point-ion model was first introduced by Gourary and Adrian[32] and has been improved and extended both by these authors[33] and Laughlin[34]. To discuss this model, we may start with the Hartree-Fock equation for a one-electron wavefunction

$$[p^2/2m + V(\vec{r})]\ \Psi_i(\vec{r}) = E_i\Psi_i(\vec{r}), \qquad (3.2)$$

where $\vec{r}$ represents the coordinates of the F-center electron, and $V(\vec{r})$

contains the interaction energy of that electron with the nuclei as well as its Coulomb and exchange interactions with the other electrons in the crystal. The defect wavefunctions must be orthogonal both to themselves and to the wavefunctions of the electrons on neighboring lattice atoms. Following the Schmidt orthogonalization scheme, we replace Ψ_i with Φ_i, a smoothed function orthogonalized to the eigenstates of the energy operator with the core or valence wavefunctions of ion n, Φ_{cn}. Thus

$$\Psi_i = \Phi_i - \sum_{c,n} (\Phi_{cn}, \Phi_i)\, \Phi_{cn}(\vec{r}),$$

where (Φ_{cn}, Φ_i) signifies $\int d\vec{r}\, \Phi^*_{cn}(\vec{r})\, \Phi_i(\vec{r})$, and c is a core or valence state of ion n. This substitution in (3.2) yields the modified Hartree-Fock equation

$$[(p^2/2m) + V(\vec{r})]\, \Phi_i(\vec{r}) - \sum_{c,n} (\Phi_{cn}, \Phi_i)(E_{cn} - E_i)\, \Phi_{cn}(\vec{r}) = E_i \Phi_i(\vec{r}), \quad (3.3)$$

where we have used the fact that $[(p^2/2m) + V(\vec{r})]\, \Phi_{cn}(\vec{r}) = E_{cn}\Phi_{cn}(\vec{r})$ by definition of Φ_{cn}.

In the point-ion approximation, the crystal potential is divided into contributions from the long-range, smoothly varying Madelung potential, $V_m(\vec{r})$, and a short range, wildly varying potential arising from the fact that the charge density of the F electron extends beyond the nearest-neighbor ions and experiences forces not described by the smoothly varying Madelung potential. In this approximation, both this term and the orthogonalization term are neglected and solutions are sought for the remaining equation

$$[(p^2/2m) + V_m(\vec{r})]\, \Phi_i(\vec{r}) = E_i \Phi_i(\vec{r}) \,. \quad (3.4)$$

Gourary and Adrian used a variational technique to solve this equation assuming s-like and p-like wavefunctions for the ground and excited states, respectively. Thus, these workers additionally ignored any contribution to $V_m(\vec{r})$ arising from non-spherically symmetric interactions. The wavefunctions giving the lowest energies had the form of Bessel functions inside the vacancy and were of the form $(1/r^n)$ exp $(-r/r_o)$ outside the vacancy, although simple s and p hydrogenic wavefunctions gave substantially equal results. Laughlin[34], solving (3.4) numerically has found energies for the F absorptions in several alkali halides which agree within 2% of those found by Gourary and Adrian. These transition energies fall within 10-15% of the experimentally determined values for the alkali halides treated, and the Mollwo-Ivey relation is derivable from their results. Nevertheless, the point-ion model cannot be used to obtain information on higher excited states of the F center for which the wavefunctions might extend well beyond the confines of the vacancy. It ignores lattice polarization and a large part of the ionic potential both of which would be important in such cases. Moreover, the wavefunctions computed within this approximation are not orthogonal to the valence and core states of neighboring ions.

A second approach which does not ignore the two terms set equal to zero in the previous treatment is the so-called extended-ion approximation. In this scheme, the full modified Hartree-Fock equation (3.3) is attacked with the restriction that only nearest neighbors are taken explicitly into account. Electronic and lattice polarization effects have been included in some calculations using this approximation[35], but the most extensive, by Wood and coworkers[36-38], ignored this possibility. They did, however, allow for possible displacement of nearest neighbor

ions. This was done by writing the Madelung energy as two terms, one involving the smooth potential from all of the crystal but the six nearest neighbors, and a second involving the potential of the nearest neighbors at an adjustable position, R_i. The total energy of the F-center electron in their case may be written as

$$E_F = KE - (a_m - 6)\, R_o^{-1} - \sum_{i=1}^{6} R_i^{-1} + A_i + \Delta + E_{ex} + E_{ov},$$

where KE is the kinetic energy, the second and third terms are the Madelung terms already discussed, A_i is the small Madelung correction term ignored in the point-ion treatment, Δ is a negative correction term arising from the fact that the F electron penetrates the core orbitals of the nearest neighbor ions a small fraction of the time and does not experience the full screening effect of these electrons, E_{ex} is the exchange energy and E_{ov} is the energy due to orthogonalization, also neglected earlier. For calculation of the integrals contained in this expression, a simple radial wavefunction $\phi = r^n \exp(-\beta r)$ was chosen, since the results of Gourary and Adrian had indicated that the minimum energies obtained did not depend sensitively upon the exact form of the wavefunction used. In the wavefunction above, n = 0, 1 or 2 and β is an adjustable scaling parameter.

To obtain the transition energy for the F center, the total energy of a perfect crystal containing an F center and six displaced nearest neighbors was minimized with respect to R_i and β, and the value of E_F required by the values of these parameters computed. Because E_F itself was contained in the energy expression being minimized, this was an iterative process. Then, assuming that the electronic transition involved in absorption of a quantum of energy would occur so rapidly that

the positions of the ions would not change during the transition, they calculated a new value of E_F for an excited state wavefunction using the same values of R_1 and β which minimized E_F for the ground state. The difference of these two values of E_F, of course, gave the absorption energies for the F center. The approximation involving the time in which electronic transitions take place relative to the motion of the lattice ions is called the Franck-Condon principle and will be utilized in later sections of this chapter.

The agreement of the Wood et al. results with experimentally determined values was somewhat better than those of Gourary and Adrian, and their calculations were extendable to the excited states of the F center. The distortions of the nearest-neighbor ions were found to be 1% or less. Recently, Wood has used this scheme to discuss the theoretical basis of the Mollwo-Ivey relationship in some detail[38].

The Width of the F Absorption--The Configuration-Coordinate Model

We shall discuss the widths of the F and other absorptions at finite temperatures first using the simple configuration coordinate model which illustrates many of the physical principles involved, and then shall expand our discussion to include more recent work not suffering many of the limitations imposed by this model.

The Schrödinger equation for a solid may be schematically written as

$$[T_e + T_N + U(\vec{r},\vec{R})]\,\Psi(\vec{r},\vec{R}) = E\Psi(\vec{r},\vec{R}), \qquad (3.5)$$

where T_e and T_N are the kinetic energies of the electrons and nuclei

which are at positions schematically given by $\vec{r}$ and $\vec{R}$, and $U(\vec{r},\vec{R})$ is the total potential energy function for the entire crystal and contains electron-electron, electron-nucleus, nucleus-nucleus and spin interactions. The eigenstates of the electrons depend upon the value of this total potential energy; however, because they are capable of following the detailed motion of the lattice ions, the potential which they feel is essentially set only by the nuclear coordinates. In a vibrating lattice, therefore, the eigenstates of the electrons change continuously and adiabatically as the nuclei move. On the other hand, the nuclei respond only to the average positions of the electrons, since they are not capable of following the detailed motion of the electrons. Thus, the electrons move in a potential dependent only upon the nuclear coordinates and the nuclei move in a "potential" which is actually the energy eigenvalue of the electrons. This is the content of the important adiabatic or Born-Oppenheimer approximation[39]. Because of this consideration, the solution of (3.5) may be written as a product wavefunction $\Psi_{nN}(\vec{r},\vec{R}) = \Phi_{n,R}(\vec{r})\, X_{nN}(\vec{R})$, where n and N are the set of electronic and nuclear quantum numbers, $\Phi_{n,R}(\vec{r})$ is the electronic wavefunction which depends parametrically upon the instantaneous value of the nuclear coordinates $\vec{R}$, and $X_{nN}(\vec{R})$ is the nuclear wavefunction, which depends only upon the electronic quantum numbers and not upon the electronic coordinates. Thus, the individual wavefunctions should separately satisfy the equations

$$[T_e + U(\vec{r},\vec{R})]\, \Phi_{n,R}(\vec{r}) = E_n(\vec{R})\, \Phi_{n,R}(\vec{r}),$$

and

$$[T_N + E_n(\vec{R})]\, X_{nN}(\vec{R}) = E_{nN}\, X_{nN}(\vec{R}) .$$

This latter equation is normally treated in the harmonic approximation in which $E_n(\vec{R})$ is expanded about nuclear equilibrium only through second-order terms. Under these conditions, this equation becomes similar to that for a set of harmonic oscillators, and the X_{nN} are the set of wavefunctions obtained for the quantum mechanical harmonic oscillator problem.

The probability per unit time that an atom will make a transition from state g to state e is proportional to the square of the dipole matrix element $\vec{r}_{eg}$ connecting the two states[40], where

$$\vec{r}_{eg} = \sum_s \int \Psi_e \vec{r}_s \Psi_g \, d\tau \, . \qquad (3.6)$$

The sum is over all electrons in the atom, Ψ_e and Ψ_g are solutions to the time-independent Schrödinger equation, and the integral is over all electronic coordinates. Our "atom" in this case is simply an anion vacancy containing a single electron, and the "crystal" we need to consider for now consists of this F center and as many of the surrounding nuclei as may be necessary to determine the potential energy of the electron. For the simple model we are going to use, the nearest neighbor ions are the only ones considered[40-45]. With these vast simplifications, and within the adiabatic approximation, the dipole matrix element takes on the factored form

$$\vec{r}_{eg} = \int \Phi_{e,R}(\vec{r}) \, \vec{r} \Phi_{g,R}(\vec{r}) d\tau \int X_{e,J}(\vec{R}) \, X_{g,K}(\vec{R}) d\tau,$$

where we have allowed for the possibility that the nuclear overlap integral may depend upon both the electronic and nuclear energy states. Because the first integral depends only parametrically upon the nuclear

positions, it cannot set the energy of the transitions but only the relative probability of the electronic transition for each value of R for given e and g. This integral is therefore proportional to the oscillator strength for the transition. Only the second integral can affect the actual energy of the transition, and it does so through dependence of the electronic energy eigenvalue upon $\vec{R}$, and secondarily upon J and K. These dependences can be visualized on a diagram if we assume that the F center energy states are sensitive to some simple, single vibrational mode and can, therefore, be represented against a single coordinate--the configurational coordinate, Q. This single mode is usually chosen to be the totally symmetric breathing mode of the nearest neighbors. Figure 7 shows the variation of the total energy of the system with Q for the ground and first excited states. In the harmonic approximation, the curves are parabolas. Discrete electronic levels arising from different values of the nuclear quantum numbers J and K are shown within the classical parabolic limits.

Immediately, we may qualitatively see the reason for several experimental observations. First, because the quantum-mechanical probability function for the ground state of an harmonic oscillator is a Gaussian peaking at Q_g, the absorption band should peak at the energy represented by the arrow labeled Abs, and should be essentially Gaussian itself, if the curvature of the excited-state potential may be neglected. Second, within the Franck-Condon approximation already discussed, there should be a difference between the peak energies of the absorption and emission bands. The most probable absorption would occur vertically from the equilibrium position of the ground state, while the most probable emission would occur vertically from the equilibrium position of the excited

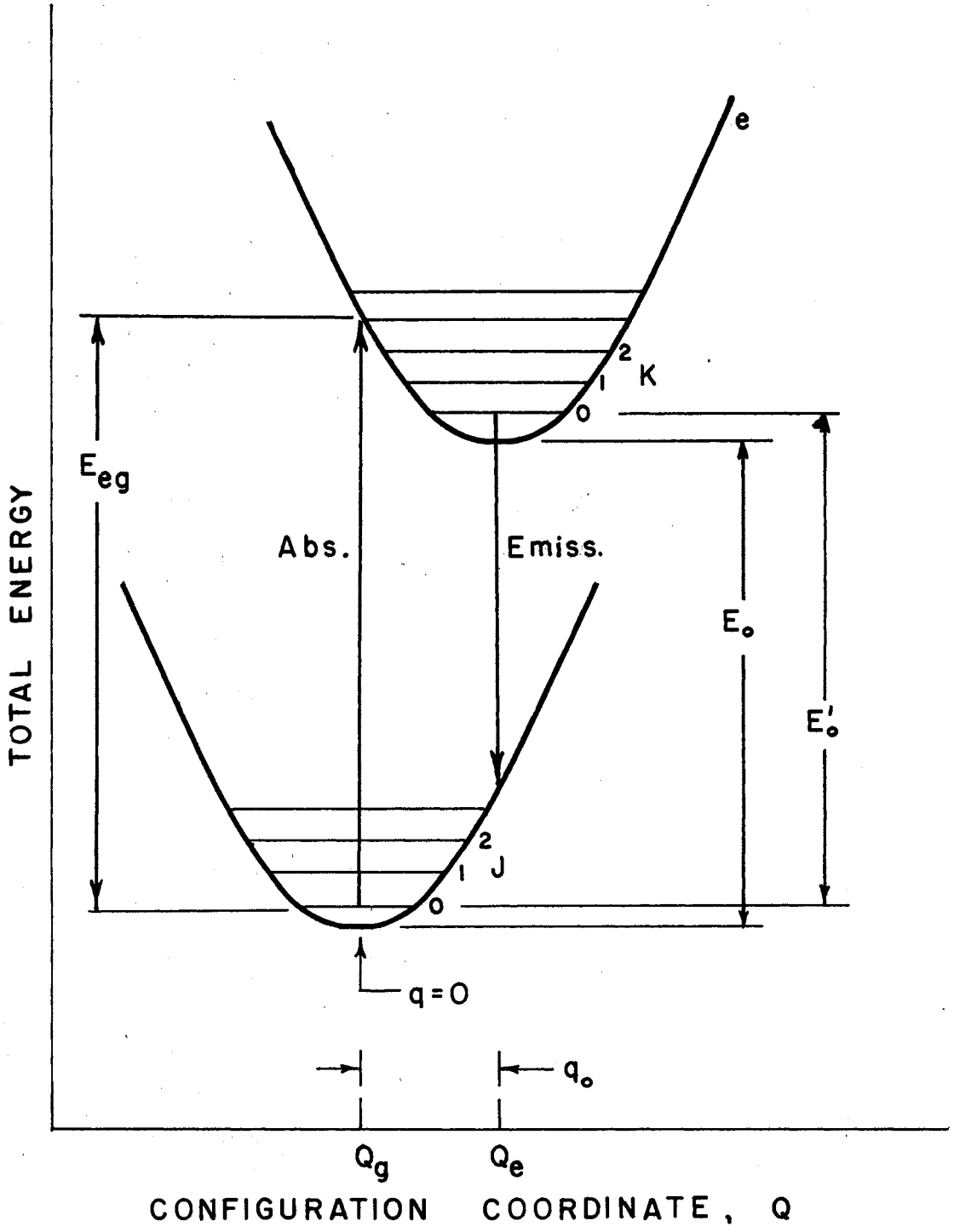

Figure 7. The Configuration Coordinate Diagram

state. This is the origin of the Stokes shift. Third, at low temperatures where only the lowest energy ground state J = 0 is populated, there should occur with some probability a transition from J = 0 to K = 0 in which no vibrational quantum change is involved. This zero-phonon transition is observed in many systems. Because the wavefunctions for the ground state of the system takes the form of a damped exponential outside the solid curve, we might expect the probability of observing such a transition to depend upon the separation $Q_e - Q_g$ in the same way. We shall presently see that this is the case.

Let us now examine the model more formally and obtain some relations which will be useful in interpretation of the data obtained on F_2 centers in this work. In terms of displacements q about $Q = Q_g$, the ground state of the totally symmetric normal mode of the harmonic oscillator can be written $E_g = \frac{1}{2} M \omega_g^2 q^2$, where M is the effective mass, and ω_g the frequency of the mode. We have set E = 0 at $Q = Q_g$. The energy of the excited state, classically, is $E_e = E_0 + (q - q_o)^2 \frac{M \omega_e^2}{2}$, where we have assumed that M does not change, but have allowed the frequency of the normal mode dominant in the excited state to differ from that for the ground state. Expanding, this becomes

$$E_e = E_o + \tfrac{1}{2} q_o^2 M\omega_e^2 + \tfrac{1}{2} q^2 M\omega_e^2 - q q_o M\omega_e^2$$

$$= E_{eg} + \tfrac{1}{2} q^2 M\omega_e^2 - Aq,$$

where we have used the fact that $E_{eg} = E_o + \frac{1}{2} q_o^2 M\omega_e^2$ and have set $q_o M\omega_e^2 = A$, a constant which measures the sensitivity of the relaxation of the nearest neighbor ions to the energy of the electron in its excited state. To obtain an expression for the absorption energy of this

system, we treat the excited state classically because the transition is to levels for which the spacing of the vibrational levels can be ignored, and the ground state quantum mechanically because the transition arises, at low temperatures, from levels near J = 0 for which the spacing of vibrational levels cannot be ignored. Writing the ground state energy as the zero-point value, $\frac{1}{2}\hbar\omega_g$, we obtain

$$\Delta E_F = E_{eg} - \tfrac{1}{2}\hbar\omega + \tfrac{1}{2}q^2 M\omega_e^2 - Aq \ . \qquad (3.7)$$

Now, for perfectly parabolic energy curves, the probability as a function of energy for a transition from the ground state to an excited state is simply the probability of finding the system at a coordinate q in the ground state times a Jacobian to take account of the change of variable from displacement to energy. For the harmonic oscillator, this is[46]

$$P(E) = [(M\omega_g^2)/(2\pi kT)]^{\frac{1}{2}} \exp [(-M\omega_g^2 q^2)/(2kT)](dq/dE). \qquad (3.8)$$

At low temperatures, however, this is erroneous, because the ground state energy is far from being described by the classical parabola[47]. Williams and Hebb[48] show that the correct semiclassical relation is identical to (3.8) with T replaced by an effective temperature,

$$T_{eff} = \left(\frac{\hbar\omega_g}{2k}\right) \coth (\hbar\omega_g/2kT) \ .$$

The Jacobian may be evaluated from (3.7). When this is done, and the halfpeak points evaluated, the full width at half-maximum is seen to be

$$H(T) = H(0)\,[\coth(\hbar\omega_g/2kT)]^{\frac{1}{2}}, \tag{3.9}$$

where H(0) is the low-temperature limiting value of H(T), given by

$$H(0) = [(4\ \ln 2)(\hbar/M\omega_g)]^{\frac{1}{2}} M\omega_e{}^2 q_o .$$

In order to introduce the Huang-Rhys factor S in a natural way, let us approach the problem once more in the same approximation. But this time, we shall treat both the ground and excited states of the harmonic oscillator quantum mechanically. From our discussion of the adiabatic approximation, it is apparent that the width of the absorption line will depend only upon the overlap integral between the ground and excited state harmonic oscillator wavefunctions. The wavefunctions required will be those with energy eigenvalues for the ground and excited states of

$$E_{gJ} = (J + \tfrac{1}{2})\hbar\omega, \text{ and } E_{eK} = (K + \tfrac{1}{2})\hbar\omega + E_{eg} - S\hbar\omega \tag{3.10}$$

where this time the quantum-mechanical expressions for the energy have been used instead of the classical ones used earlier, and a dimensionless coupling constant S has been introduced to express the strength of the interaction which displaces the equilibrium position of the excited-state mode. In this treatment, commonly referred to as that of linear coupling, the mode frequency is not allowed to differ in the ground and excited states. Keil[49] has calculated the overlap integral between such displaced harmonic oscillator wavefunctions, and obtained

$$\langle X_{eK} | X_{gJ} \rangle = \exp(-S/2)\,[\tfrac{J!}{K!}]^{\frac{1}{2}}\, S^{\frac{1}{2}(K-J)}\, L_J^{K-J}(S),$$

where $L_J^{K-J}(S)$ is the Laguerre polynomial. The normalized transition probability from the ground to the excited state, is, then

$$W_{KJ} = |\langle X_{eK}|X_{gJ}\rangle|^2 = e^{-S}\left[\frac{J!}{K!}\right] S^{(K-J)}\left[L_J^{K-J}(S)\right]^2 .$$

At T = 0, the only ground-state level occupied is that for J = 0. The function $L_0^K(S) = 1$, and $W_{K0} = (S^K/K!)\exp(-S)$. From Equations (3.10), it can be seen that the spectrum at T = 0 is a series of lines at $E_K = (E_{eg} - S\hbar\omega) + K\hbar\omega = E_0' + K\hbar\omega$.

These would be weighted in intensity by W_{K0}. The zero-phonon line at energy E_0' is seen to have the normalized probability $W_{00} = e^{-S}$; that is, the probability of seeing a zero phonon transition for a center decreases as a damped exponential as S increases. This result was anticipated from our earlier qualitative examination of Figure 7. Practically speaking, no zero-phonon line is likely to be observed experimentally for $S \gtrsim 6$.

At finite temperatures, levels with J > 0 become thermally populated. If we introduce an index p = K-J which indicates the net number of vibrational quanta involved in the transition, we see from Equations (3.10) that the absorption spectrum at finite temperatures is once again a series of lines at energies $E_p = E_o' + p\hbar\omega$. The normalized probability for the transitions in this case, however, must be determined by performing a thermally weighted average over the initial ground states. Keil obtains for this thermally averaged probability

$$W_p = \exp\left[(p\hbar\omega)/(2kT) - S\coth\left(\frac{\hbar\omega}{2kT}\right)\right] I_p\left[S\coth\left(\frac{\hbar\omega}{2kT}\right)\right], \quad (3.11)$$

where $I_p(z)$ is the Bessel function of the first kind with imaginary

argument. The width of these individual transitions would be, on this model, limited only by the lifetime of the states. In practice, line widths for the zero-phonon line are some four orders of magnitude larger than this, due presumably to random lattice strain[50].

It is apparent from Figure 7 and the second of Equations (3.10) that $S\hbar\omega$ is simply the energy above the K = 0 level that the absorption maximum occurs. The numerical value of S, then, can be interpreted as the number of phonons involved in the most probable absorption transition. In the linear coupling approximation, the shapes of both the ground and excited state functions are identical, and the energy difference between the absorption and emission transitions shown in Figure 7 will be simply $2S\hbar\omega$. This is the Stokes shift to be expected between the absorption band for a system and the corresponding luminescence band in the linear coupling approximation.

Using (3.11) the expression for the absorption half width as a function of temperature is found to be

$$H(T) = H(0)\ \mathrm{csch}\ \left(\frac{\hbar\omega}{2kT}\right),$$

which is indistinguishable from (3.9) in practice. For the very-nearly Gaussian band shape predicted by (3.11) at high temperature[43], we obtain

$$H(0) = 2.36\ S^{\frac{1}{2}}\hbar\omega\ . \qquad (3.12)$$

The Huang-Rhys factor for a broad-band transition may be evaluated from (3.12) if an experimental measurement of H(0) is available and if ω can be determined in some way. The latter can be done using measured values of H(T) for T > 0. Equation (3.9) can be fit to measured values

of H(T), using the value at T = 0 for H(0). Better, a plot of arc coth $[H^2(T)/H^2(0)]$ vs 1/T should yield a straight line through the origin for the proper choice of H(0). The slope of the line, $\hbar\omega/2k$, then may be used to obtain ω. Although the latter is the more powerful method it is quite sensitive to small thermometry or optical errors. For data with significant scatter, the former is often the more practical method of obtaining values for H(0) and ω, and hence, for S.

The energy of the peak of many absorption bands shifts with temperature. Most absorptions tend toward higher energies at low temperatures, but no satisfactory quantative theory exists for the effect. Recent work by Gilbert and Wood[51] indicates that the major part of the effect is due to the change in the lattice constant with temperature, as might be expected, but that there are other contributions to this shift which have not yet been elucidated.

It is possible to fit half-width data to plots such as have been discussed in this section, and consequently to determine a value for ω, for a large number of centers of different types in many different host lattices. The question arises, that if the configuration coordinate treatment with its rather crude assumptions is so imperfect, why is it so often possible to fit the data to an expression such as (3.11) and obtain a value of ω? Moreover, one of the most glaring errors in the quantum-mechanical model is the assumption that the same mode interacts with both the ground and excited states, even though the excited-state wavefunctions have different symmetries by their very nature and should be expected not to interact strongly with the same modes as the ground-state wavefunctions. Yet, values of ω_e determined by fitting emission data to expressions similar to (3.11), only differ from values of ω_g for

the same center by a few percent in many cases. We may find a partial answer to these problems by noting that these various types of centers introduce local and resonant lattice modes, depending upon their relative masses. Because of ω's found often are not those of known phonon branches, it may be that local modes are the principal ones interacting with the centers, or that the frequency found is some weighted average of those for several interacting lattice modes. Moreover, lattice or local modes tend to pile up near certain frequencies. For this reason, it might not be surprising, even if the ground and excited states do interact with completely different lattice modes, that similar effective frequencies are found. Markham[43] has considered these interpretational problems in some detail. The real value of this treatment lies not so much in the accuracy of the parameters obtained, but in its hueristic value in color-center research and in the fact that a marked deviation of behavior of some center from that predicted by the configuration-coordinate model may well indicate a new physical effect.

In the quantum mechanical configuration coordinate model all transitions with the same value of $p = K-J$ were degenerate, since only one lattice mode of a single frequency ω was considered. In actuality, for a center which is coupled somewhat to all of the crystal modes, one obtains, for $p = 1$, a full set of transitions reflecting the one-phonon density of states of the lattice at that temperature. Similarly, for $p = 2$, the two-phonon density of states spectrum is obtained, and so on. The broad-line spectrum seen at any temperature is then the envelope of the individual one-, two- ... phonon absorption spectra. This idea forms the basis of recent work by Mostoller, Ganguly and Wood[52]. These workers present a scheme to perform a spectral decomposition of experi-

mentally measured absorption bands to obtain the effective one-phonon density of states for the crystal. They then use this one-phonon spectrum to obtain contributions from n-phonon processes which give discernible vibronic structure and use conventional moment analysis[53] to obtain information on higher-n processes. They take account, as has been done[43,49], of the fact that other than linear coupling may exist between the ground- and excited-state interactions with the lattice modes. The fit of their predicted band shapes and other parameters with experimental data on one of the F_4 centers in NaCl is excellent. This same approach has more recently been applied to the C_{2h} F_2 center in MgF_2 with similarly good results. In this case, even the location and bandshape of the luminescence band associated with this center were predicted accurately[54]. The fact that relatively sophistdicated machine calculations are involved in their technique might seem to lessen its usefulness as a simple means of comparing properties of similar centers in a system of crystals--at least for the present average researcher. Nevertheless, this technique offers new insight into the basic processes which broaden absorption bands in solids.

Absorption Positions and Band Shapes of F_2 Centers

In one view, the F_2 center is just two adjacent F centers with shared electrons. It is perhaps not surprising, therefore, to find that several of its main electronic transitions absorb in the same energy range as the F center. There are three first-excited state transitions of this center. The lowest-energy has its transition moment aligned with the long (z) or σ axis of the center and is a $^1\Sigma_g^+ \rightarrow {}^1\Sigma_u^+$ transition in molecular notation. In an LCAO picture, this may be thought of as a

transition by the two F centers to an excited state consisting of a linear combination of 1s and $2p_z$ states. The other two transitions are of the type $^1\Sigma_g^+ \rightarrow {}^1\Pi_u^+$ and involve combinations of 1s separately with $2p_x$ and $2p_y$ states. These transitions occur along axes perpendicular to the z axis of the center often referred to in the literature as π axes. In later work, we shall denote the polarization of the transitions as simply the σ and π absorptions. In many materials, such as the alkali halides, the π_1 and π_2 transitions occur at slightly different energies, since the immediate environment of the center is different in its x and y directions. One test of the usefulness of a particular approach to calculation of the location of the F_2 transitions is its prediction of the sign and energy splitting of these two π transitions.

Theoretical investigations into the peak positions of the various F_2 absorption and emission bands have been conducted by several investigators. Herman used the model of a hydrogen molecule embedded in a continuous dielectric and obtained the transition energies by simply scaling the computed energy versus internuclear separation curves to the known vacancy separation[55]. It is not surprising that this model gave only approximate results. Evarestov[56], in a point ion approach, calculated transition energies for KCl which agreed surprisingly well with the actual values. He used hydrogenic trial wavefunctions, and a variational technique to minimize the energy. His results may have been fortuitous, since Meyer and Wood[57] point out that his trial wavefunctions fail to predict the proper transition energy for the F center. These latter authors carried out an extended ion calculation for LiCl and LiF using wavefunctions explicitly found to give the best transition energies for the F center[37]. These wavefunctions were orthogonalized

to nearest-neighbor ion states and the general calculational scheme already outlined for their F-center work.

Their calculated energies for the σ F_2 transitions were within 10% of the experimentally determined values for both salts. No values for the π transitions were available for comparison. Their method has the promise of being able to deal with the higher excited states of the F_2 center. Because the π splittings are clearly dependent upon the details of the nearest neighbor distortions--not allowed for in any of these schemes--it is doubtful that great success in predicting this splitting will be enjoyed even by the extended ion treatment for F_2 centers.

The width of the absorption band of the F_2 center can be treated on a configuration-coordinate model little different from the one discussed earlier. One need only allow for three first-excited state energies corresponding to the three molecular states possible for that state of the center. Mostoller and coworkers, as noted, have calculated the broad band absorption and emission properties of this center in MgF_2 with good success[54].

CHAPTER IV

RADIATION DAMAGE IN ZnF_2

In Chapter I, the two principal radiation damage processes were outlined. In this chapter, we shall present optical absorption data for ZnF_2 bombarded with 2 MeV electrons as a function of the temperature of irradiation. From these data, we shall attempt to identify the predominant radiation damage process active in ZnF_2, and suggest tentative identifications for the various absorption bands which occur upon irradiation of this material. Finally, a more detailed damage mechanism will be presented and discussed in relation to that proposed for MgF_2 by Sibley and Facey[17], and by Buckton and Pooley[58].

Experimental Procedure

Crystals of ZnF_2 from boule 081971 were cut on (110) faces with the c axis in the plane of the specimen. The samples ranged in thickness from 0.05 to 0.11 cm and were oriented and polished as described in Chapter II. These samples were irradiated with 2 MeV electrons from a Van de Graaff accelerator at the Oak Ridge National Laboratory. Three different controlled temperature irradiation devices were employed during the course of the experiments. For the low temperature work, two essentially identical fixed-point cryostats manufactured by the Sulfrian Cryogenic Corporation were used. Above ambient, a small furnace capable of holding the sample temperature constant at temperatures up to 200°C

was employed. In the cryostat used for measurements at 15, 80, 145, 235, and 280 K, a gold:0.7 atomic % iron vs chromel P cryogenic thermocouple indicated the temperature. A platinum resistance thermometer was the temperature indicating element in another cryostat used at 205 K and for a second set of irradiations at 15 K. The boiling points of He, N_2, Freon 14, and Freon 22 were used for the irradiations at 15, 80, 145, and 235 K respectively. Heating of the sample by the electron beam was responsible for the differences between the measured temperatures and the known boiling points of these fluids. The irradiations at 205 and 280 K were accomplished using dry ice-acetone and ice-water slurries, respectively. The oven used for the two high temperature measurements was designed so that optical sample holders could be inserted directly in it, and employed a copper vs constantan thermocouple to indicate temperature. For all irradiations, the samples were positioned 15.0 cm from the exit port of the accelerator. Uniform coverage of the samples by the electron beam was insured by scanning the beam over the samples in a square raster during the irradiations. Beam intensities were held constant to ±5%, and the accumulated dose was indicated by an electromechanical charge integrator. Therefore, the exact value of the beam current was relatively unimportant. Beam intensities of 5 μA, measured as the total current striking the constant-temperature holder, were employed for all irradiations but those at 15, 320 and 370 K. Because it was impossible to keep the sample temperature at an acceptable value when a higher beam current was used, the intensity was reduced to 1 μA for the liquid helium temperature irradiations. Even so, a steady state temperature of 15 K was the lowest obtained even with the lower current. For irradiations at 320 and 370 K, a beam intensity of 10 μA was employed. The

fraction of the beam current which actually fell on the sample surfaces is known to within approximately 30% for the cryostat runs, and only to within 100% for the high temperature runs. This dosimetry information was provided by E. Sonder of the Oak Ridge National Laboratory, and was accomplished using silver-doped phosphate glass dosimeters[59]. It was verified using Faraday cups or the rate of heating of suitably-masked blocks of potassium chloride.

Optical spectra were recorded over the range from 1.77 - 6.70 eV (700 - 185 nm) on a Cary model 14 spectrophotometer. Of course, optical measurement temperatures of the samples irradiated in the cryostats were at the fixed temperatures of the various baths employed and not at the slightly higher irradiation temperatures. Spectra for the 320 and 370 K irradiation temperatures were taken at room temperature. The spectrum of a typical unirradiated crystal of ZnF_2 is presented in Figure 8. In it, the absorption coefficient, α, is plotted as a function of the energy of the incident photon. A wavelength scale is provided at the top of the figure for reference. The optical absorption coefficient is defined as the natural logarithm of the ratio of incident to transmitted intensities per unit path length. Because most dual beam spectrophotometers record the base-ten log, this is usually written as $\alpha = (2.303/t) \log_{10} (I/I_o)$, where I and I_o are the intensities of the optical beam respectively after and before passing through a sample of thickness t. The quantity $\log_{10} I/I_o$ is called the optical density (O.D.).

Radiation Damage Growth Curves

Figures 9 and 10, plotted in a similar manner to the last figure, but with the unirradiated crystal spectrum subtracted, illustrate the

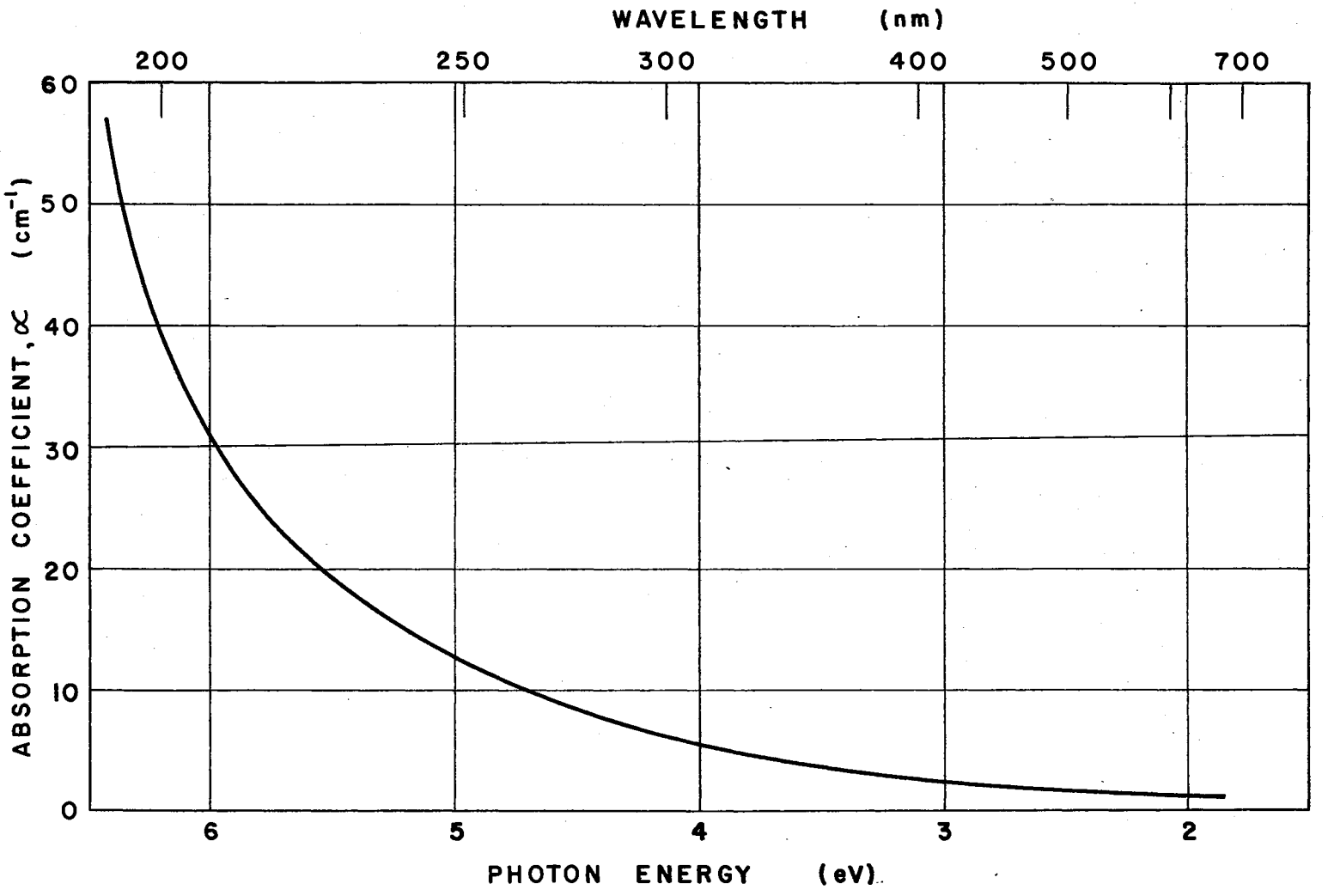

Figure 8. Optical Absorption of Unirradiated ZnF_2

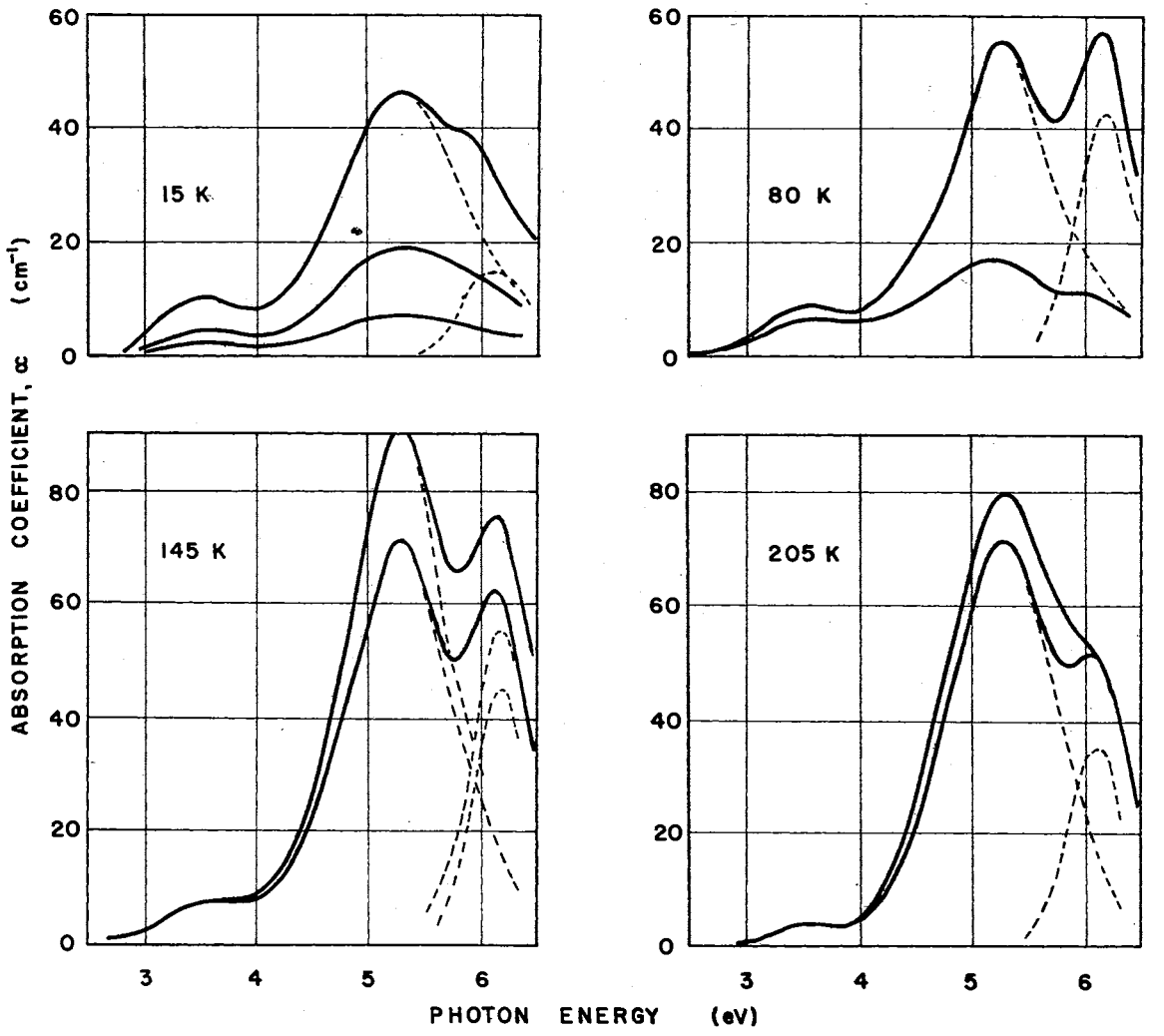

Figure 9. Optical Absorption of ZnF_2 Irradiated at 15, 80, 145 and 205 K for Low and High Doses

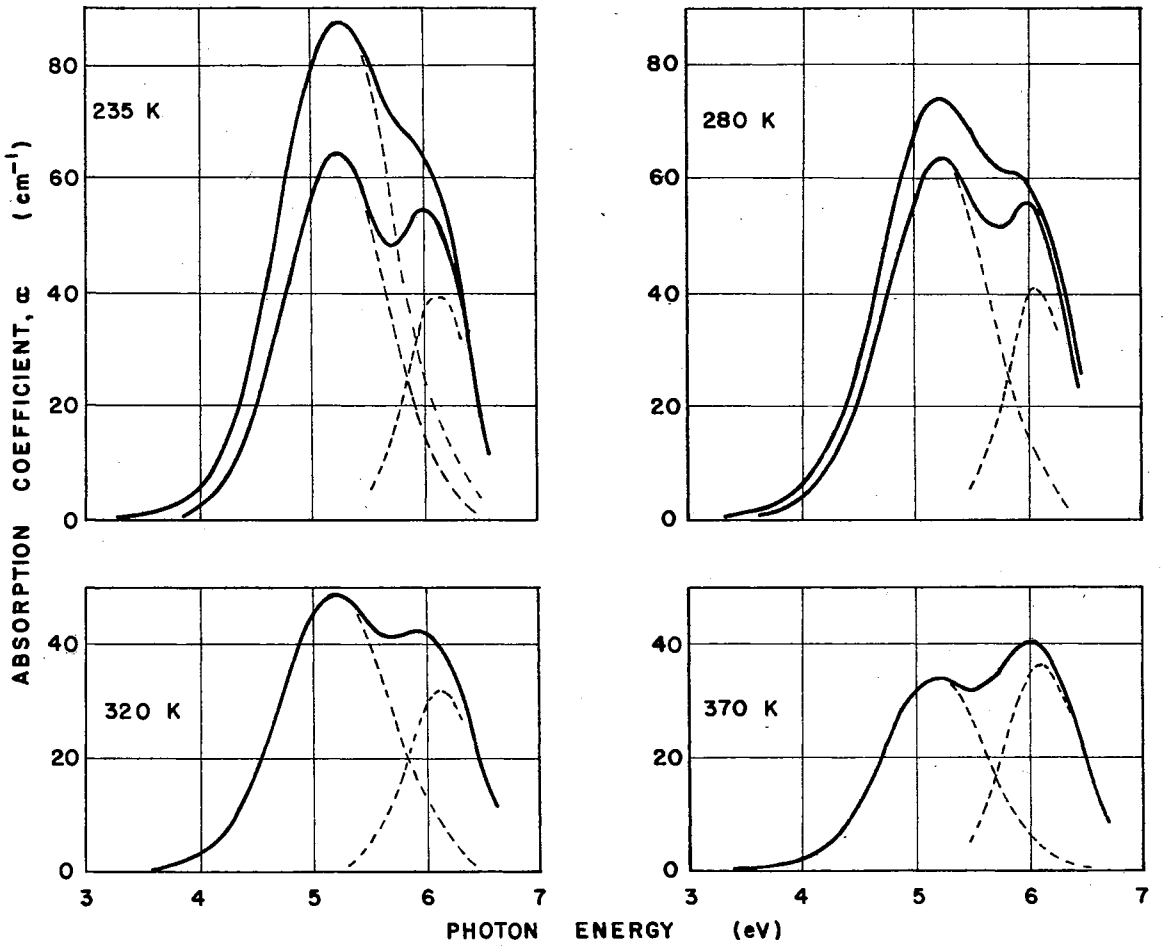

Figure 10. Optical Absorption of ZnF_2 Irradiated at 235, 280, 320 and 370 K for Low and High Doses

optical absorption found in ZnF_2 for relatively low and for high electron doses at the eight temperatures employed. Three absorption bands are evident. The one peaking near 3.5 eV (350 nm) appears in all samples irradiated at 205 K and below, but not in any specimens irradiated above this temperature. It grows in quickly and saturates at a low value of absorption coefficient. Such behaviour is reminescent of that for the $[F_2^-]$ center in alkali fluorides, but no positive identification of this band could be made under the circumstances extant during the radiation damage growth experiments. The broad band peaking near 5.2 eV (240 nm), and that near 6.1 eV (205 nm) are the only other obvious features of the spectra; however, high resolution plots of the data taken at low doses at 15 K show possible unresolved structure at energies between 5.5 and 6.0 eV.

Also shown as dashed lines in Figures 9 and 10, are decompositions of some of the spectra into their component bands. This is only an approximate decomposition and was accomplished in the following manner: the peak position of the 5.2 eV band was assumed to be at the apparent value read from the plots. Using this peak position, the lower-energy half of this band was replotted onto the upper-energy side, yielding a symmetric approximation to the entire band. This band was then subtracted from the spectrum to obtain the 6.1 eV band. From these curves, the approximate peak positions and full widths at half maximum for each band was read and are tabulated in Table I. It is apparent that the half widths of both bands are significantly larger at 15 K than at higher temperatures. It should be noted that the spectra of the two highest temperature irradiations were taken at room temperature, while the other spectra shown were measured at the fixed points used for the

TABLE I

PEAK POSITIONS AND FULL-WIDTHS AT HALF MAXIMUM FOR THE 5.2 AND 6.1 eV ABSORPTIONS IN ZnF_2

Irradiation Temperature (^oK)	Measurement Temperature (^oK)	Peak Position of 5.2 eV Absorption (eV)	Half-Width of 5.2 eV Absorption (eV)	Peak Position of 6.1 eV Absorption (eV)	Half-Width of 6.1 eV Absorption (eV)
15	7	5.28	1.34	6.12	0.65
80	78	5.26	1.10	6.17	0.58
145	142	5.25	1.12	6.15	0.56
205	195	5.23	1.14	6.12	0.56
235	232	5.22	1.15	6.13	0.53
280	273	5.21	1.16	6.08	0.54
320	300	5.19	1.12	6.12	0.76
370	300	5.15	1.08	6.08	0.78

irradiations. It is not apparent from the table, but for any one irradiation temperature, the half widths found for both bands tended to be progressively greater for progressively greater band heights. This effect is probably due to growth of other centers under these major ones.

From data in the table, it is apparent that the half-width of the 5.2 eV band does not change significantly from 80 through 380 K. The half-width of the 6.1 eV band, however, appears to increase considerably as the temperature is increased. The peak positions of both bands appear to shift toward lower energies at higher temperatures.

From the decomposed spectra, it is evident that the 6.1 eV band saturates in its growth at optical densities of 30 - 40 cm^{-1} for irradiation temperatures of 205 K and above; however, at the three lowest temperatures, this band is still growing at the highest doses used. The 5.2 eV band also tends to saturate for irradiation temperatures of 205 K and above. From the decomposed spectra, it is apparent that this band tends not to saturate at as low a dose as the 6.1 eV band. The difference in saturation doses, however, is small, and it is not entirely safe to conclude that the two bands arise from different centers. Nevertheless, from the available data, this is the more likely prospect.

Figure 11 presents the growth of the 5.2 eV band with radiation dose at the temperatures employed. The optical absorption at the peak of the band is plotted against the total absorbed dose expressed in MeV/cm^3. The band at 6.1 eV has not been subtracted out, but as Figures 9 and 10 show, its width is such that its contribution under the peak of the 5.2 eV band is negligible for all cases. The temperatures in ^{o}K for each irradiation are shown beside the appropriate curve. The measured growth curves fall into two broad categories: those at 15 and 80 K are

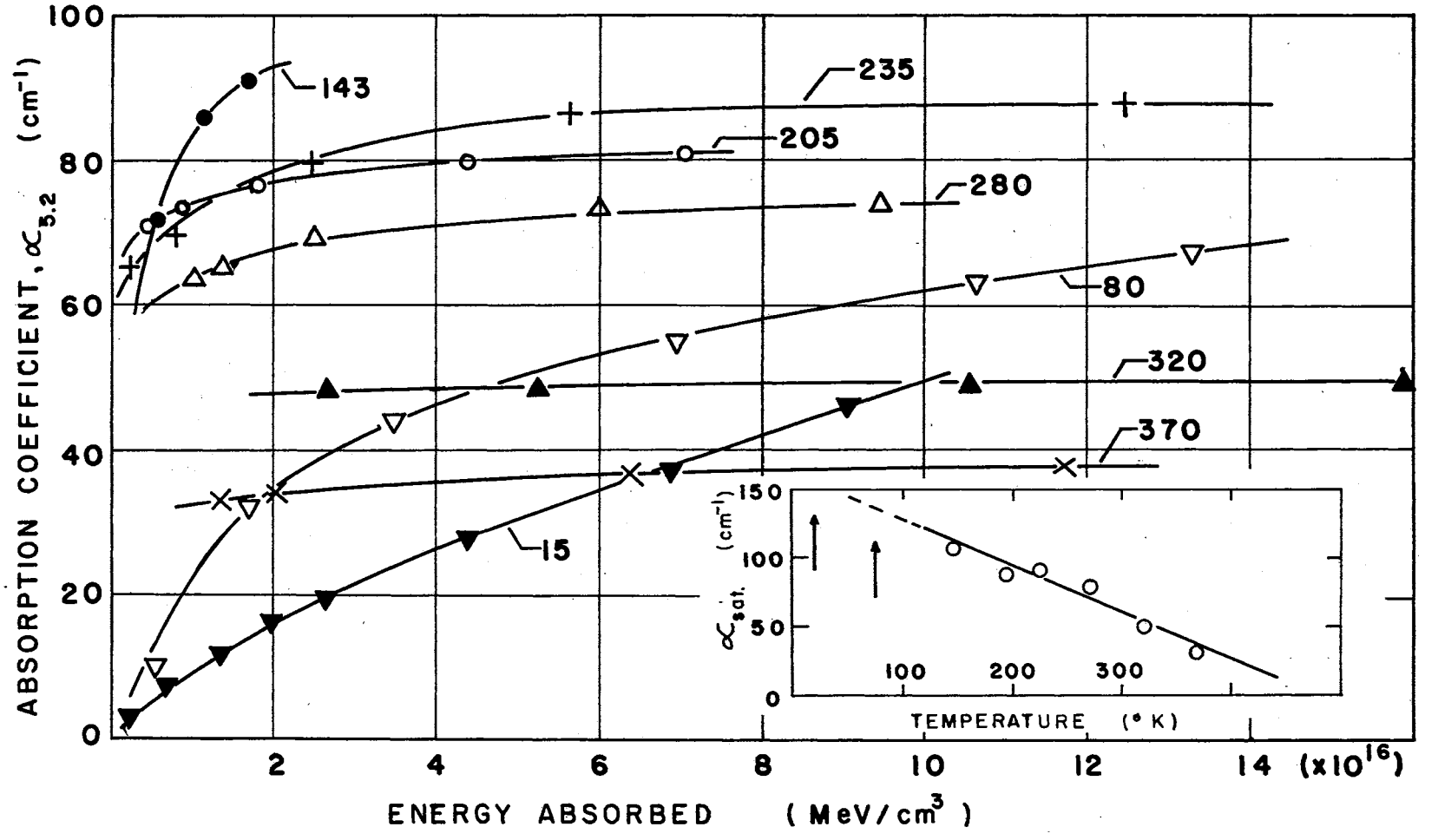

Figure 11. Growth of the 5.2 eV Absorption in ZnF_2 With Irradiation at the Temperatures Shown. The Inset Shows the Saturation Value of Each Curve Versus the Absolute Temperature

similar and show a slowly saturating behavior, while those at higher temperatures show a rapidly saturating growth. Because of the difficulty in comparing the fluxes actually falling on the samples for the different irradiations, the exact shape of the initial rapidly-growing portions of each curve should be taken only as a rough indication of the actual behavior of the material in this dose range.

The inset in Figure 11 shows the saturation value of the absorption coefficient at the peak of the 5.2 eV band vs absolute temperature of irradiation. Because the 15 and 80 K curves never reach saturation, only an arrow has been shown at these temperatures. It is evident that their saturation values will be considerably above those of the other curves, and that the saturation value of the 15 K curve will be higher than that for the 80 K curve. This observation is reflected in the placement of the arrows in the inset.

Discussion

In Chapter I, the elastic collision and photochemical damage mechanisms were briefly outlined. Let us now discuss these mechanisms in more detail and attempt to discover which of them is the predominant one in ZnF_2.

It is not the purpose of this preliminary study of the radiation damage in ZnF_2 to unambiguously associate a particular optical absorption band with each radiation damage center expected. So that we may more conveniently discuss the data, however, it is expedient to tentatively identify the absorption at 5.2 eV as either arising from an F center or interstitial. That it belongs to the F center will be asserted on the grounds that it lies at about the expected energy compared to

other materials. If subsequent work reveals that the 6.1 eV band is actually the absorption associated with the F center, or if the two absorptions are later found to arise from the same center--F or interstitial--no qualitative changes should have to be made in the interpretations given here.

For an incident particle or photon to cause elastic or knock-on damage, it is necessary for it to impart enough energy to a lattice ion to displace it into a nearby interstice--typically 10 - 30 eV. For a relativistic electron, the maximum energy which can be imparted to a lattice atom or ion is $T_{max} = 2(E + 2mc^2)\ E/Mc^2$ where E is the electron energy and m and M are the masses of the electron and lattice ions. For a 2 MeV electron striking a fluorine atom, T_{max} is 684 eV. Thus, in principle, knock-on damage is possible for the irradiations carried out in this work. Calculations by Oen[60] for displacement cross sections of lattice atoms in solids predict a primary cross section for fluorine under bombardment by 2 MeV electrons of 30 - 40 barns, that is, $3 - 4 \times 10^{-23}$ cm^2. Because the incident electrons may make many more than one elastic collision before being stopped or leaving the crystal, the damage cross section, when secondaries are included, rises to a value nearer 7×10^{-23} cm^2 [60]. For a known flux of electrons, the concentration of defects to be expected from knock-on damage is $N = N_o\ \phi\sigma_d$ where N is the number of defects per cm^3, ϕ the integrated electron flux, σ_d the total displacement cross section, and N_o the number density of fluorine atoms in ZnF_2. The density of F atoms in ZnF_2 can be calculated from its molecular weight and mass density to be 5.4×10^{22} fluorine atoms/cm^3.

For the lowest irradiation dose employed at 80 K, the integrated electron flux on the sample, ϕ, was approximately $5 - 7 \times 10^{14}$ electrons/

cm^2. Using the larger values for each of these quantities in the expression above, an upper limit to the concentration of interstitials expected from knock on damage is found to be $3 \times 10^{15}/cm^3$. Because one vacancy is made for every interstitial created, this is also the expected upper limit for the number of F centers. It is an upper limit not only because the largest reasonable values of the various parameters have been used, but also because it assumes no recombination of interstitials and vacancies under the influence of the radiation. In order to compare this expected upper limit to the concentration of F centers actually found, we may call upon the well-known equation which relates the peak height of a given optical band to the concentration in the crystal of the centers responsible for that band. This equation, due to Smakula[61], and corrected slightly by Dexter[62] may be written for a gaussian band as

$$fN = 0.87 \times 10^{17} \frac{n}{(n^2 + 2)^2} H\alpha_{max}$$

where f is the oscillator strength for the transition giving rise to that band, n is the index of refraction of the material, H is the full width at half maximum for the band and α_{max} is the value of the optical absorption coefficient at the peak of the band. Utilizing the measured values of the various parameters, and assuming f to be unity to obtain a lower limit on N, the F center concentration at the first data point for the 80 K irradiation is 1.1×10^{17} cm^{-3}--a value considerably higher than the 3×10^{15} cm^{-3} expected for knock-on damage. Thus, it is clear that this mechanism cannot account even for the concentration of defects generated by the irradiations at 15 K, and certainly not for the concen-

tration found at 145 K.

We are led, then, to expect a photochemical damage process to be operative in ZnF_2. Such a process has previously been determined by Sibley and Facey[17] to be active in MgF_2. These workers found that the energy to create a single F center in that material in the early stages of damage was approximately 2×10^4 eV near room temperature and nearer 1×10^5 eV at 80 K. Buckton and Pooley[58] have measured this same quantity as 4×10^5 eV at 80 K. Again, using the data from the lowest data point taken at 80 K, we may estimate this number for ZnF_2. First, however, it is necessary to determine the energy which each electron imparts to the lattice as it passes through the crystal. The range of a 2 MeV electron in ZnF_2 can be computed to be very nearly 2.0 mm[63]. This is commensurate with the experimentally measured ranges for MgF_2 and KCl, if the differences in mass density are taken into account. Since the energy deposited per unit distance traveled is constant for all but the last few per cent of the electron path[63], and since none of the crystals used were as thick as 2 mm, the energy deposited by each electron may be closely approximated as 2 MeV times the ratio of the thickness of the crystal to the range. This relation was used to establish the abscissa scale for Figure 11. Using the value calculated above for the F center concentration near the first data point at 80 K, the energy required to create one F center in ZnF_2 at 80 K is seen to be approximately 6×10^4 eV. At 145 K, the energy to create one F center has dropped to near 1×10^4 eV. It is wise to be cautious in attaching significance to F-center production energies at the higher temperatures, since it is known for alkali halides and MgF_2 alike that small amounts of impurities can markedly affect this quantity at low doses[9,10,17,64].

The two anions in an $[F_2^-]$ center are considerably closer together than are two normal lattice ions[14]. When the self-trapped hole is annihilated by an electron, an electrostatic recombination energy approximately equal to the band gap of the material is released, most of which becomes available to produce recoil of the two anions toward their normal lattice positions[14]. For a given recoil energy, the efficiency with which these recoiling ions can create stable Frenkel pairs at low temperatures should depend to a large extent upon the ease with which the recoiling ion or atom can slip between its neighbors into an interstice. This should be dependent in turn upon details of the path required to arrive at an interstice; that is, upon the crystal structure of the material. For materials of the same structure, it should further depend upon the relative crowding of the ions which make up the lattice; that is, upon the size of the opening through which the recoiling ion or atom must pass. At finite temperatures, the stability of the Frenkel pairs would depend sensitively upon their initial separation, and some have felt that a mechanism capable of producing widely separated pairs, such as the focusing replacement sequence discussed in Chapter I, was necessary for successful operation of the Pooley mechanism[11-13]. This work, and that on MgF_2 already referenced, would seem to show that such is not the case in some materials: Magnesium fluoride and ZnF_2 possess no obvious focusing directions, yet damage photochemically. No obvious mechanism exists to separate the vacancy and its interstitial great distances; nevertheless, stable damage is found at low temperatures. One might expect, therefore, that stable pairs of F centers and interstitials having very small separations might be possible in these materials.

Let us now consider a more detailed picture of the radiation damage

mechanism in ZnF_2, and compare it to ones proposed for MgF_2 by the authors mentioned above. Figure 12, taken from reference 17, presents F center growth curves for irradiation of MgF_2 by 2 MeV electrons. These data are analogous to those presented in Figure 11 for ZnF_2. From the figure, it can be seen that MgF_2 damages relatively more at both low and high temperatures than at intermediate ones. In fact, no damage could be produced by these workers at 145 K even after prolonged irradiation. A relatively simple model has been presented qualitatively by Sibley and Facey, and more rigorously by Buckton and Pooley to explain the observed growth patterns of the F center in MgF_2. In Figure 13 is shown an idealized plot of the potential existing in the MgF_2 lattice along a zig zag path passing from interstice to interstice. It is apparent from qualitative consideration of the figure that three regimes should exist in which the damage process would differ. At very low temperatures, such as at 4 K, any damage created would be stable, since the temperature would not be sufficiently high to allow an interstitial to return to the vacancy even from the next-nearest interstice, marked B. At slightly higher temperatures, however, correlated jumps back into the vacancy could begin to occur under the influence of the radiation, so that radiation-enhanced recombination would exist during irradiation to compete with the production process. This would explain the observed lower production rate of F centers at intermediate temperatures. Still no radiation diffusion of interstitials over the barrier E_3 could take place until even higher temperatures were reached. When this diffusion began to take place, one would expect the production rate to once again increase, since now many of the interstitials would be able to diffuse away from their associated vacancies before recombination took place.

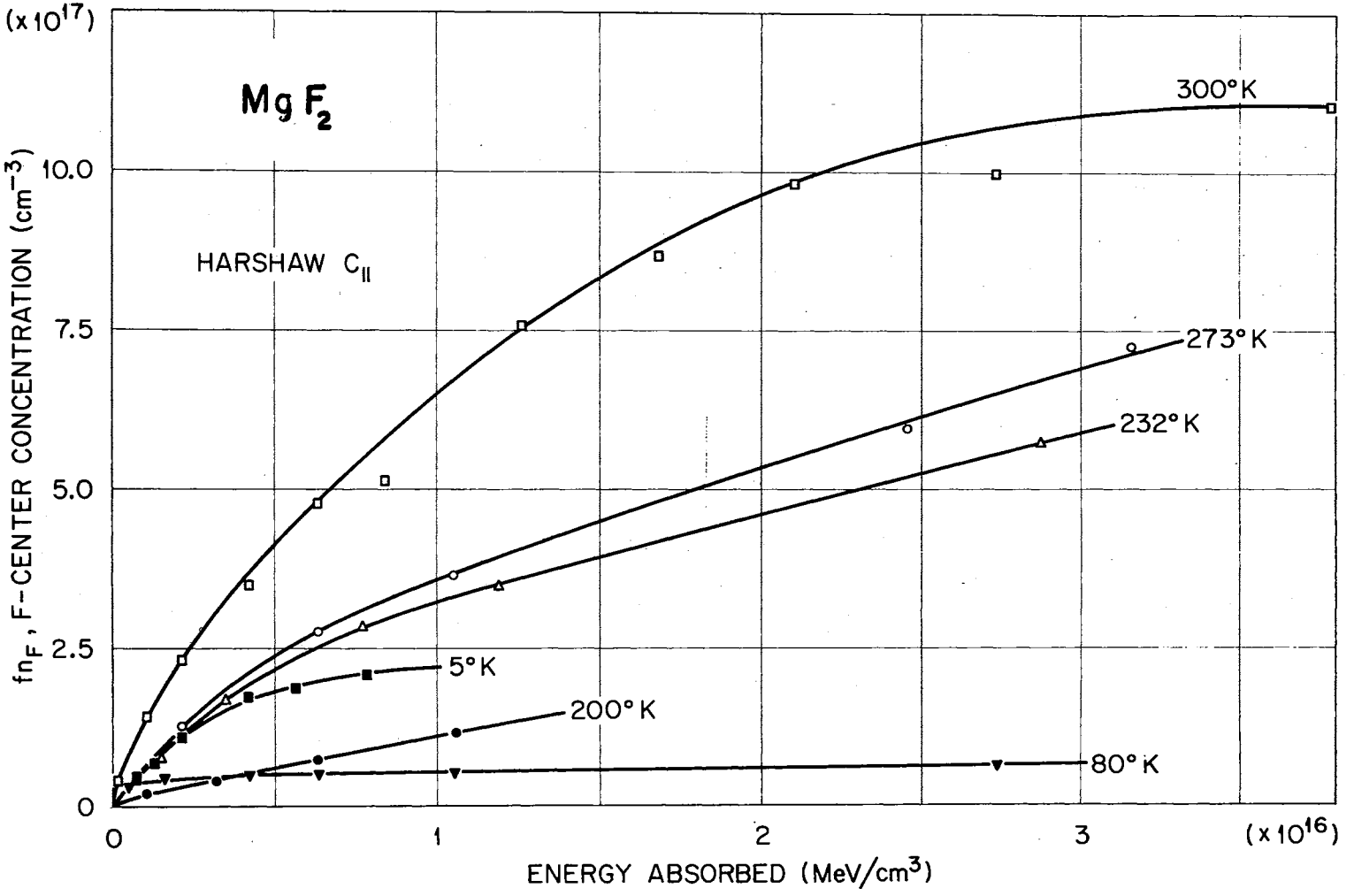

Figure 12. Growth of the F Band in MgF_2 With Irradiation at the Temperatures Shown

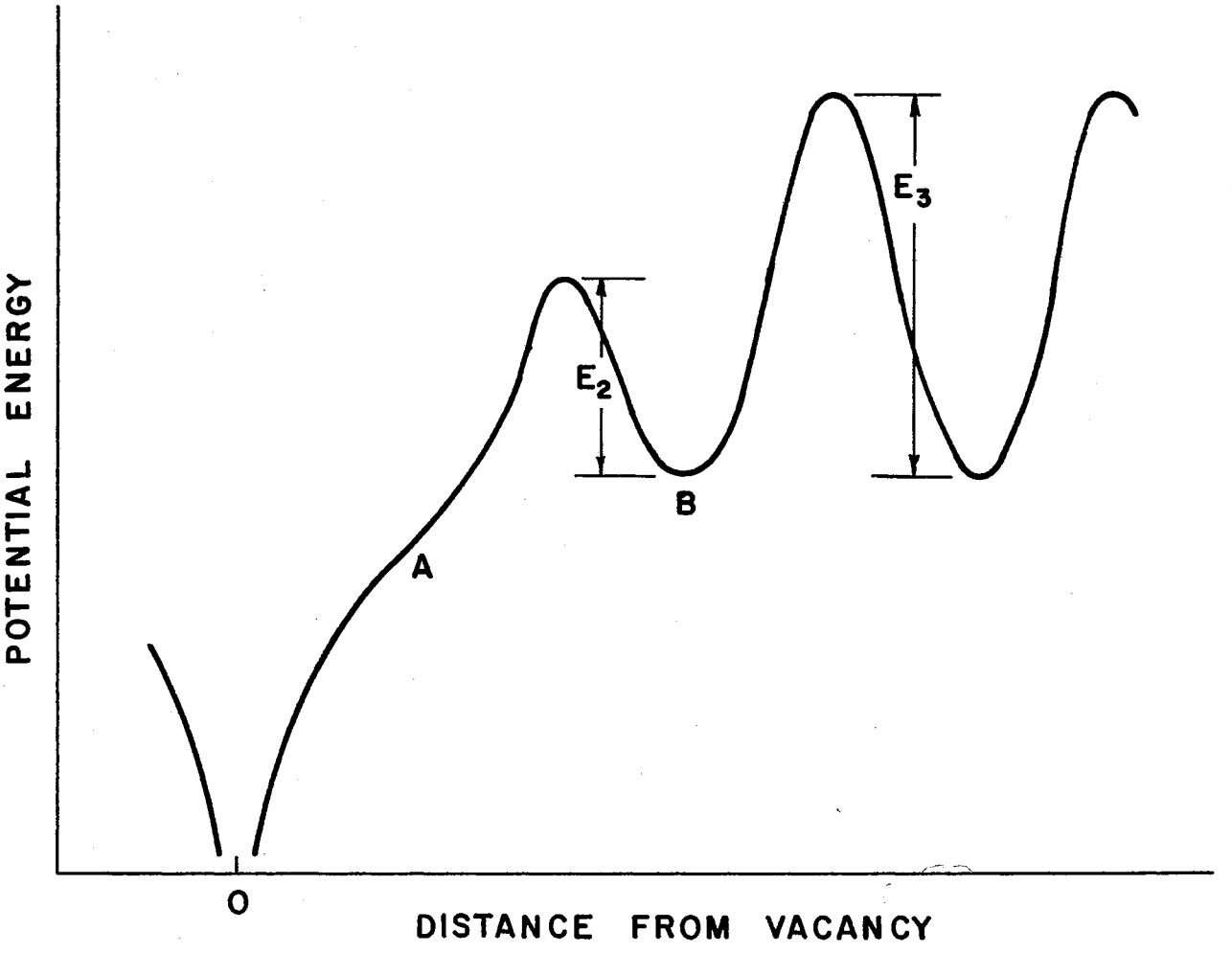

Figure 13. Schematic Representation of Potential Energy Versus Distance From the Vacancy in MgF_2

Following Buckton and Pooley, we may put these qualitative ideas on a quantitative basis for MgF_2. One F center is produced for each interstitial made. We shall label an interstitial existing at any but the closest distance from a vacancy with the symbol S, because it would result in separated F center and interstitial. An interstitial existing at the closest distance, however, we shall label as P to indicate that it is part of an F center-interstitial pair, even though the experimental evidence is that these both appear as one absorption[58]. The rate of production of close interstitials, then, would be

$$\frac{dP}{dt} = k_p I - k_r I\ P \exp(-E_2/kT) - k_d I\ P \exp(-E_3/kT), \qquad (4.1)$$

while the rate of production of isolated interstitials or F centers would be

$$\frac{dS}{dt} = k_d\ P\ I \exp(-E_3/kT)\ . \qquad (4.2)$$

This assumes that no interstitial is produced by the radiation directly into any but the closest interstice. Here k_p, k_r, and k_d are the rate constants for production, recombination and dissociation, respectively. The temperature dependences of k_r and k_d have been written explicitly; no temperature dependence of k_d is assumed. Linear dependences of each process upon the radiation intensity, I, is assumed here. The work of Buckton and Pooley indicates that this is a correct assumption. From these equations, we obtain

$$P = \frac{k_p}{A}\left[1 - \exp(-AIt)\right]$$

where $A = k_r \exp(-E_2/kT) + k_d \exp(-E_3/kT)$ and where the constant of integration has been evaluated from the fact that $P = 0$ at $t = 0$. Using this expression for P, we find

$$S = \frac{k_p IB}{A} \{t + \frac{1}{AI} [1 - \exp(-AIt)]\}$$

in which $B = k_d \exp(-E_3/kT)$, and the constant has been evaluated using the fact that $S = 0$ at $t = 0$. The experimental evidence is that both of these centers appear as one absorption. The observed concentration of F centers, then would be

$$F(T) = P + S = \frac{k_p}{A} \{[1 - \exp(-AIt)] + BIt - \frac{B}{A} [1 - \exp(-AIt)]\} \quad (4.3)$$

For MgF_2, we assume $E_2 < E_3$, and investigate three temperature regimes: $T \sim 0$, $T \sim \infty$, and an intermediate regime in which radiation enhanced diffusion allows recombination over the barrier E_2 but not over E_3.

Case I. Low Temperatures

Here both A and $B/A \sim 0$. We may ignore the last two terms in 4.3, and expand the exponential, yielding

$$F(0) = k_p I t \quad (4.4)$$

Thus, at low temperature, we expect intensity dependent, non saturating growth.

Case II. High Temperatures

For this case, the exponentials of A and B would all approach unity,

and the ratio B/A would approach $k_d/(k_r + k_d)$. Then,

$$F(\infty) = \left(\frac{k_d\, k_p}{k_r + k_d}\right) It + \left(\frac{k_p - k_d}{k_r + k_d}\right) \{1 - \exp\,[-It(k_r + k_d)]\} .$$

At high temperatures, the probability would be great that every interstitial made would move away from its vacancy so that $k_d \approx k_p$. If this obtained, the second term would approach zero and the first term would become, as at low temperatures,

$$F(\infty) = k_p\, I\, t \qquad (4.5)$$

Case III. Intermediate Temperatures

In this regime, $B/A \sim 0$ but A is no longer negligible. The second two terms of (4.3) may still be neglected, and we are left with

$$F(III) = \frac{k_p}{A} [1 - \exp\,(-AIt)] . \qquad (4.6)$$

In this range of temperature, the growth is intensity independent, and saturating. Further, the saturation level would decrease with temperature due to the exponential in the denominator. These results are all in qualitative agreement with those shown in Figure 12.

Two pieces of correlative information are presented in references 17 and 58 which lend credance to this model for MgF_2. The first involves annealing behavior of the F-center absorption in samples irradiated at 4 K and subsequently warmed to room temperature. Sibley and Facey observed that the F centers completely disappeared under such treatment, indicating that they were indeed made very close to their corresponding interstitial center. When the temperature was raised to values at which

one of the centers--presumably the interstitial--could diffuse easily, the anticenters annihilated, leaving an undamaged crystal. An apparent difference was observed for ZnF_2. The concentration of F centers created under irradiation at 15 K remained virtually unchanged when the sample was warmed to room temperature. A maximum change of perhaps 10% in the height of the 5.2 eV band was observed in one sample treated in this way, and no detectable change was observed in another. The first sample still had over 60% of its F centers even after storage for 90 days in room light--a treatment which could easily have caused optical bleaching of the F centers as opposed to thermal annealing.

The second coorborative observation was presented by Buckton and Pooley who noted that the full width at half maximum for the F center in MgF_2 was different in crystals irradiated and measured at 4 K, and in those irradiated at higher temperatures and measured at 4K. They attributed this difference in half widths to the presence under the F band of another absorption due to F centers perturbed by nearby interstitials. These centers were presumed not to exist in samples irradiated at temperatures where such close pairs were not stable. It may be seen from Table I that the 5.2 eV band in ZnF_2 shows a similarly anomalous half width of 1.34 eV when measured at 4 K after irradiation at 15 K. A half-width measurement of the F center absorption at 4 K of the sample irradiated at 280 K yielded 1.06 eV--a value in keeping with those found at 80 K and above. Thus, whatever the explanation for the effect noted in MgF_2, a similar one would be suggested for ZnF_2. It might seem difficult to reconcile the explanation of the above authors with the observed lack of annealing in ZnF_2. If no centers anneal between 15 and 300 K in ZnF_2, it would be hard to imagine that the reduction in half width of the

F band were due to annihilation of any close pair centers. It is true, however, that quite a small absorption located to one side of a larger one can significantly alter the apparent half width of the larger. It is possible, then, that a small number of centers--the close pairs--could have disappeared as the ZnF_2 samples irradiated at 15 K were warmed without this loss being reflected by any gross change in the peak height of the F band.

Examination of the F center growth curves for ZnF_2, Figure 11, reveals that the simple picture presented to explain the damage of MgF_2 is somewhat inadequate for ZnF_2. It can explain the essentially nonsaturating behavior of the growth at 15 K, and the saturating growth at higher temperatures. It can even explain the absence of the highest temperature characteristic growth found for MgF_2 with proper choices of the ratio E_2/E_3. It cannot, however, be reconciled to the observation that the growth curve at 80 K in ZnF_2, while of the nonsaturating type, still is higher than the 15 K curve. Any recombination at all should lower the curve for 80 K. If there were no recombination at all, the 15 and 80 K curves should be identical. Moreover, even though the 145 K curve may or may not be of the nonsaturating type, it should in no case be above either the 80 K or the 15 K curves on this model.

Several other models have been considered to explain the increasing growth rates observed between 15 and 143 K. A model, for instance, in which the shoulder at A in Figure 13 actually is a potential barrier with height E_1 such that $E_1 < E_2 < E_3$ but for which E_1 is very close to the value of E_2 retains all of the desired features of the MgF_2 model, and exhibits four temperature regimes. The extra regime is one which occurs between $T = 0$ and the intermediate case considered earlier. It shows,

as needed, an increased growth rate over the T = 0 case. An assumption which seems to have a better physical basis and is far simpler, however, is that the rate constant k_p for interstitial production in ZnF_2 is temperature dependent--increasing with increasing temperature. The physical basis for this assumption lies in the recognition that ions in the ZnF_2 lattice are considerably more cramped than in the MgF_2 lattice. Scale drawings of the various interstitial passages in the MgF_2 and ZnF_2 lattices indicate that, while the interstitial passages for each are of comparable size, the ability of these passages to open up to allow passage of an interstitial is vastly different. Those in MgF_2 have considerably more ability to enlarge than corresponding ones in ZnF_2. It is likely, therefore, that the ability of a recoiling anion to force its way into an interstice would increase rapidly as the lattice expanded with temperature. Moreover, as the temperature increased, vibrational states might appear with modal patterns favoring increased interstitial channel size a significant portion of the time. A similar effect would exist in MgF_2, but if a sufficient channel size already existed, or if the ions could move apart to let the interstitial pass easily even at low temperatures, no marked temperature dependence of the damage rate in this temperature range would be observed.

CHAPTER V

F_2 CENTERS IN ZnF_2 AND MgF_2

In this chapter, we shall present and discuss measurements mainly of two types: peak position and full width at half maximum of the σ transition of the C_{2h} F_2 center in ZnF_2, and the position of the optical absorption arising from the π transition of this same center in MgF_2 and ZnF_2. The σ transition is that having its dipole transition moment oriented along the longitudinal axis of the F_2 center. There are two π transitions, perpendicular both to each other and to the longitudinal axis of the center. These transitions were discussed in more detail in Chapter III.

F_2 Centers in ZnF_2

Zinc fluoride samples used for these experiments were obtained from two sources. Samples A, B, and C were cut from a boule grown by workers at the National Bureau of Standards, Washington. The remainder were cut from boule 081971 grown by the author at this institution. All specimens but ZnF_2 C were cut with their c axes in the plane of the sample; specimen C was cut with its c axis perpendicular to the face of the crystal. We shall refer to these as $C_{\parallel}$ and $C_{\perp}$ crystals, respectively. The faces of all samples but C were (110) to within about 4° of arc; the face of sample C was necessarily (001). The F_2 centers studied were obtained by a two step process. First, a saturation level of F centers was intro-

duced into the crystal by irradiation at room temperature with 2 MeV electrons in the Van de Graaff accelerator used for the radiation damage work. F_2 centers were then introduced by bleaching the irradiated crystals for periods up to 24 hours with 254 nm light which is in the F-band region of the spectrum. Such treatment causes formation of F_2 centers in both the alkali halides and MgF_2[1,18,65,66]. The bleaching light was derived from a 250 W Hanovia mercury lamp focused with silica lenses through a Bausch and Lomb half-meter monochrometer. Because the F_2 centers in ZnF_2 and MgF_2 are oriented in unique directions by the very nature of their lattice structure, as shown in Figure 1, it was not necessary to bleach with polarized light.

Optical measurements on the F_2 centers in $c_{||}$ samples were made in a Cary model 14 spectrophotometer having Polaroid type HNP'B unsupported ultraviolet polarizers in both the sample and reference beams. These polarizers could be oriented to place the transmission direction for the electric vector of the incident light along any desired crystallographic direction of the crystal being studied. All spectra presented in this chapter have had the intrinsic absorption of these polarizers removed by subtraction. No polarizers were necessary for spectra of $c_{\perp}$ samples.

Two controlled-temperature systems were used during the course of these measurements. Those data presented for sample A were obtained with the sample mounted in a Sulfrian variable-temperature cryostat similar to the fixed point ones used for the radiation damage studies of Chapter IV. The variable temperature unit merely employed a high-impedance heat path between the cryogenic fluid and the sample. By balancing the heat input from a small electric heater against the removal of heat by the cold fluid, sample temperatures between 7 and 300 K could be obtained.

Some data points were obtained by placing hot water in the inner chamber of this cryostat. For the data presented for sample C, a Displex cryogenic refrigerator manufactured by Air Products and Chemicals, Inc., was used. With this unit, temperatures between perhaps 15 K and room temperature could be obtained and held accurately for long periods of time. Temperatures in both units were measured with thermocouples consisting of number 36 gauge gold:0.7 atomic percent iron versus Chromel P wire.

For the luminescence studies reported, light from a PEK, Inc., 75 W short-arc Xenon lamp was rendered monochromatic by a Spex Industries, Inc., one-quarter meter monochrometer and chopped at 450 Hz. The emission spectra resulting when this exciting light was allowed to fall at 45° on the face of a crystal were analyzed with a Jarrell-Ash 1 meter Czerney-Turney monochromator and detected with an RCA C-31034 multiplier phototube operated at 800 V at room temperature. The output from this phototube was conditioned by a Keithley Model 427 current amplifier and synchronously detected in quadrature by a Keithley model 840 lock-in amplifier. The detected luminescence intensity was displayed against wavelength on a Moseley model 2D X-Y recorder. Absolute calibration of the Xenon lamp was accomplished by S. I. Yun against a standard lamp having calibration traceable to the National Bureau of Standards[67].

Figure 14 presents the spectrum at 80 K of specimen A after the irradiation and bleaching described above. Absorptions of the untreated crystal and polarizers have been removed. The optical absorption coefficient, in cm^{-1}, is plotted against the energy of the incident photon for the polarizers oriented to place the electric vector, ε, of the light along the c axis ($\varepsilon \parallel c$) and perpendicular to the c axis ($\varepsilon \perp c$) of the crystal. Orientations intermediate to these yielded less anisotropy of

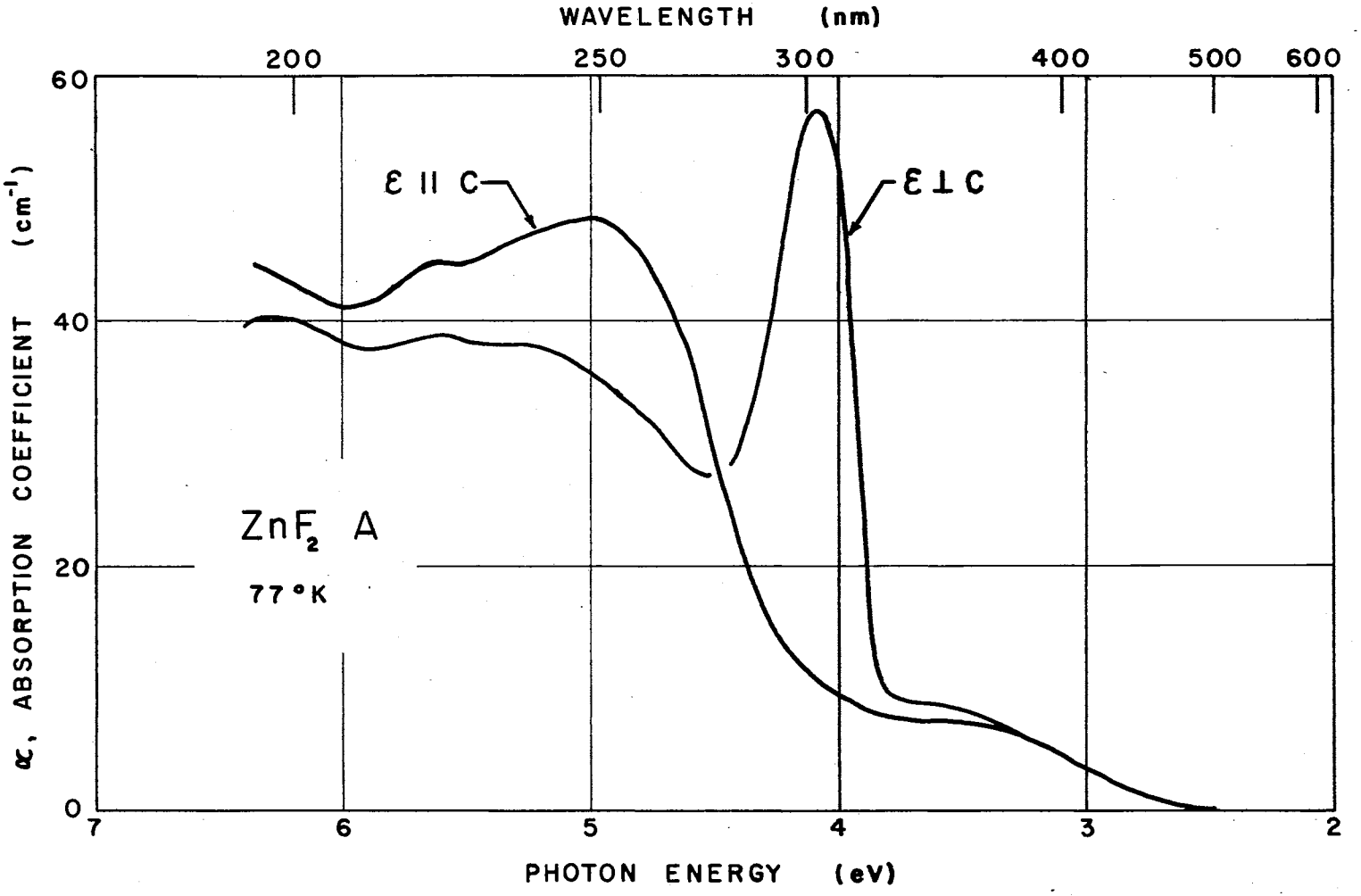

Figure 14. Optical Absorption at 80 K With $\varepsilon \| c$ and $\varepsilon \perp c$ for $c_{\|}$ ZnF_2 Sample Containing F_2 Centers

the 4.1 eV band, and revealed no absorptions not shown. The two peaks at 5.2 and 6.1 eV are clearly evident, as is the previously mentioned structure in the same region. The most striking new feature of the spectra is the highly anisotropic band with peak at 4.1 eV, and the isotropic absorption band with peak near 3.5 eV. This latter band shows no anisotropy at any measurement temperature regardless of polarizer orientation. The 4.1 eV band must arise from a center whose transition moment is oriented perpendicular to the c axis of the crystal. Figure 15 shows analogous information for a ZnF_2 sample C at 80 K. No large anisotropy of the 4.1 or 3.5 eV absorptions was found for this sample.

Figure 16 pictures the room-temperatures absorption spectrum of MgF_2 which has been similarly irradiated and bleached. This sample was obtained from the Harshaw Chemical Company for the studies of reference 65. It had previously been irradiated as described, and was bleached for this study. Again, spectra are shown for the cases in which the ε vector of the exciting light is oriented both parallel and perpendicular to the c axis of the crystal. The band with peak near 3.1 eV is totally isotropic and has been identified as arising from the F_2 center having C_1 symmetry, shown in Figure 1[66,68]. The anisotropic absorption band with peak near 3.3 eV has similarly been identified as arising from the C_{2h} F_2 center by these same workers. The D_{2h} F_2 center in this material appears only after prolonged bleaching, and is shown as a small hump at 4.2 eV on the plot of Figure 16.

In direct analogy to MgF_2, we can make the following tentative assignments: the anisotropic band in ZnF_2 at 4.1 eV evidently belongs to the σ transition of the C_{2h} F_2 center, and the isotropic band at 3.5 eV most likely arises from the C_1 F_2 center. The 4.1 eV band was

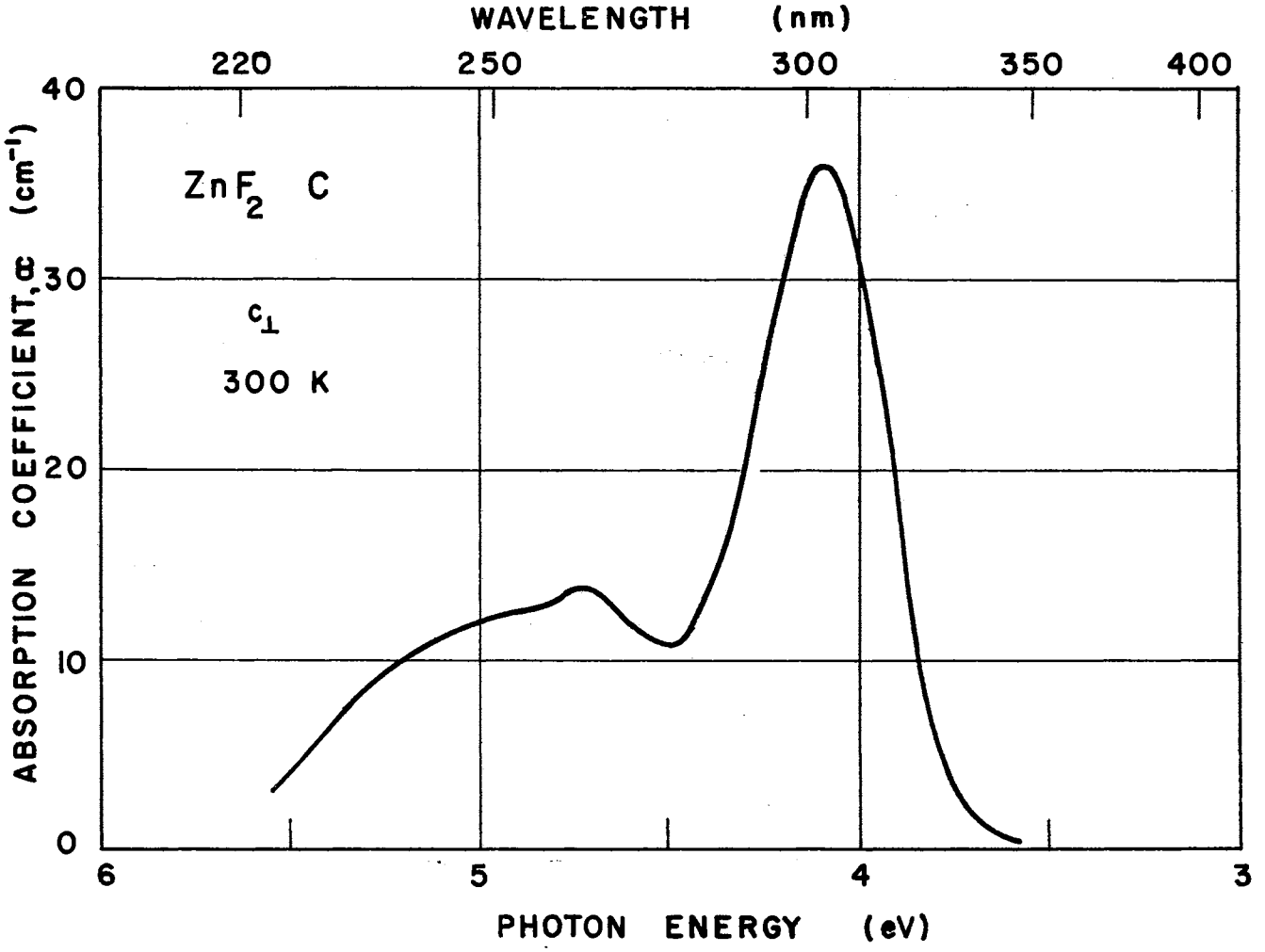

Figure 15. Optical Absorption at 80 K for $c_{\perp}$ ZnF_2 Sample Containing F_2 Centers

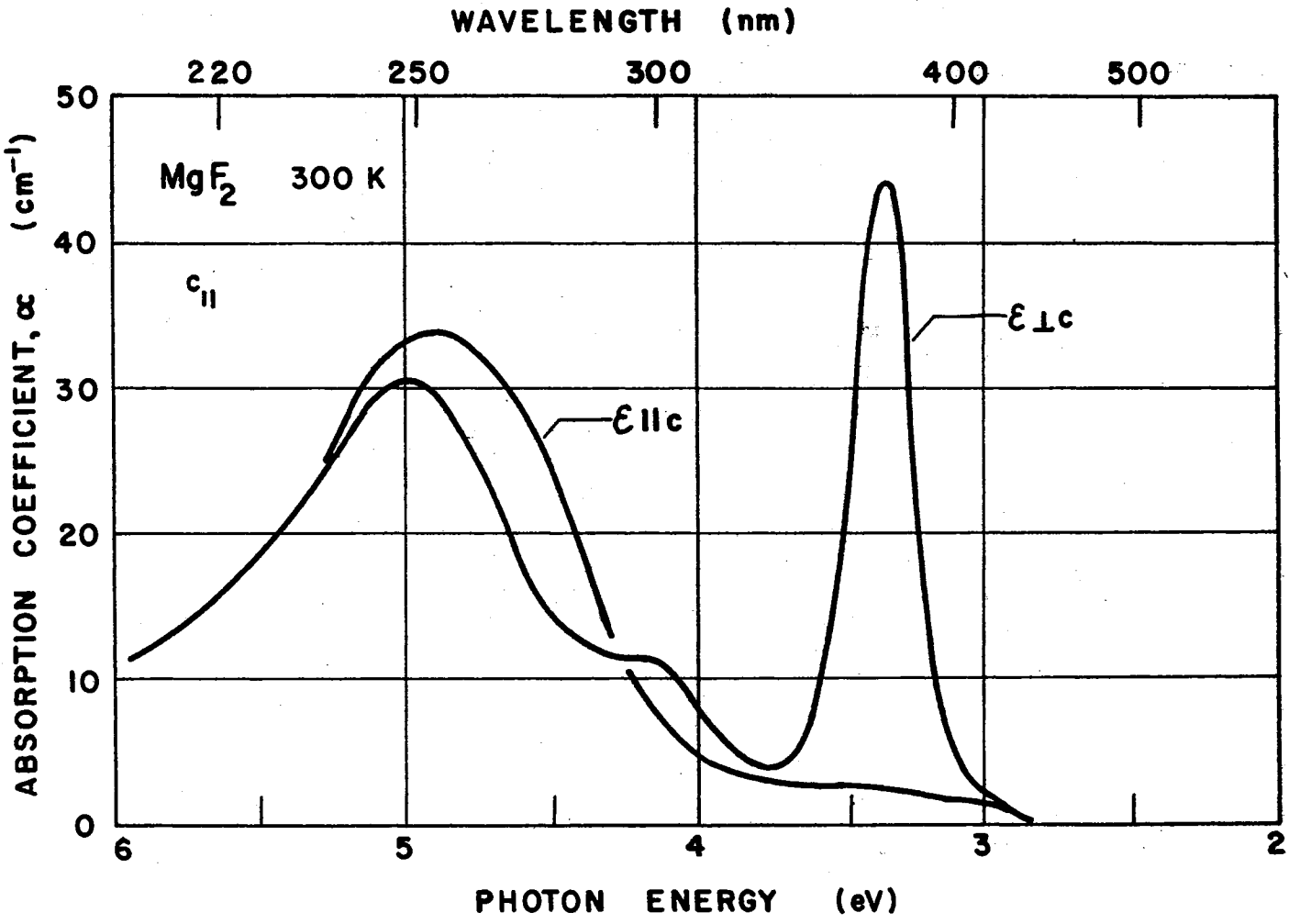

Figure 16. Optical Absorption at 80 K With $\varepsilon \| c$ and $\varepsilon_{\perp} c$ for $c_{\|}$ MgF_2 Sample Containing F_2 Centers

assigned to the C_{2h} center rather than the D_{2h} center because the latter does not appear in MgF_2 until the C_{2h} absorption has reached nearly its maximum growth. By continued analogy, therefore, the D_{2h} center is assumed not to have been made at the bleaching times used for the ZnF_2 studies. Other than this, there is no basis for the choice of one over the other, since they would have identical anisotropies in crystals cut as the ones in this study.

It might seem possible to differentiate between these two centers by a careful examination of the polarization dependence of the absorption of ZnF_2 sample C, cut with its c axis perpendicular to the face of the sample. One might expect to obtain a four-lobed polarization pattern for either center, but with the lobes pointing in different sets of directions for each. In reality, instead of a biaxial four-lobed pattern, a uniaxial two-lobed pattern oriented along a particular [110] axis was observed. Moreover, when a spectrum taken with the light oriented along a $[1\bar{1}0]$ axis was subtracted from one taken with light oriented along a [110] axis, the result was as shown in Figure 17. Not only is the anisotropic C_{2h} F_2 center present, but also the normally isotropic bands at 6.1, 5.2, and 3.5 eV. Moreover, each of these four bands appears in the figure with approximately 10% of the height it had in either spectrum alone. Because this sample showed considerable strain when later examined between crossed polarizers, it is thought that this effect most likely arises from a residual [110] uniaxial stress in the sample rather than from any innate polarization of the centers involved. The shoulder appearing near 4.7 eV will later be associated with the π transition of the C_{2h} F_2 center. It is significant that it apparently reacts to stress oppositely to the σ transition at 4.1 eV.

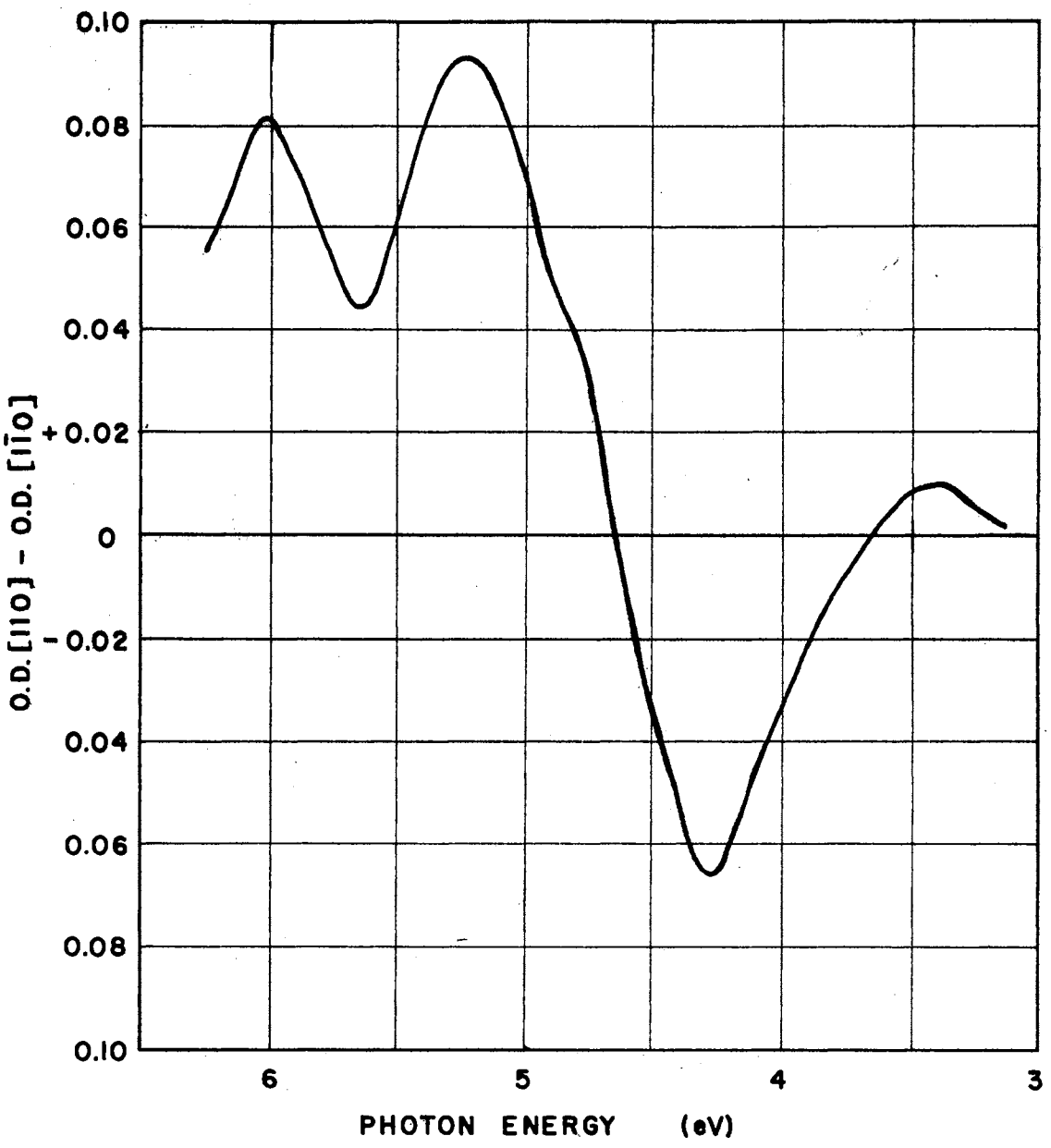

Figure 17. Difference in Optical Absorption of c_1 ZnF_2 Sample for Light Oriented Along [110] and [1$\bar{1}$0] Axes

Let us now consider the behavior of the 4.1 eV band with temperature. In Figure 18, the full widths at half maximum for this band in sample A are shown as a function of the square root of the absolute temperature. This method of presentation was discussed in Chapter III. The curve is the function $H(0)[\coth (h\nu/2kT)]^{\frac{1}{2}}$, with $H(0) = 0.41$ eV, and $\nu = 5.7 \times 10^{12}$ Hz. The data presented in the figure were read from curves obtained by subtracting the $\varepsilon \| c$ from the $\varepsilon \perp c$ spectra at each particular temperature. In Figure 19, the peak position of the 4.1 eV absorption in sample A is presented as a function of temperature. The peak of the absorption shifts toward higher energies as the temperature of the sample is increased. The full width at half maximum for the C_{2h} absorption in sample C is displayed in Figure 20 as a function of temperature. Here $\coth^{-1} [H(T)/H(0)]^2$ is plotted against the reciprocal of the absolute temperature. Again, the rationale for this type of plot was discussed earlier. The value of H(0) which gave the best straight line for these data was 0.41 eV. The slope of the resulting line, then gave a value for ν of 5.8×10^{12} Hz. These are in excellent agreement with the independent values obtained above for sample A. In MgF_2, these quantities are 0.19 eV and 8.5×10^{12} Hz[65]. The spectra obtained for sample C could not be treated in exactly the same way as those for sample A to obtain the required half widths. For a $c_\perp$ sample, there is no anisotropic behavior to reveal the true shape of the C_{2h} absorption. In this case, the known optical absorption of the F center alone must be subtracted from the spectra after suitable normalization, leaving the desired F_2 absorption.

Relying once more on information developed in Chapter III, we can now calculate the Huang-Rhys factor of the C_{2h} F_2 center in ZnF_2. The

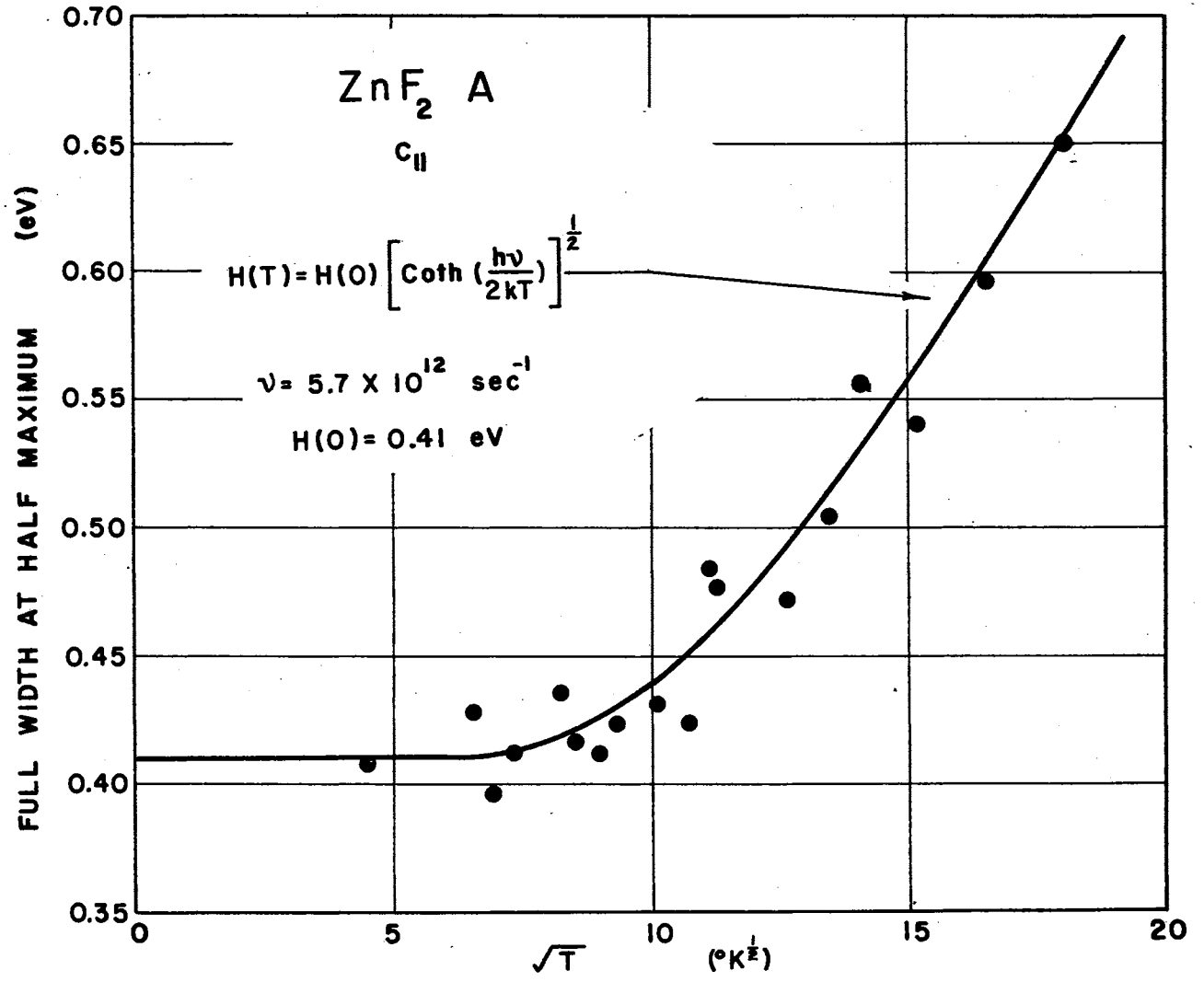

Figure 18. Half Width of C_{2h} F_2 Absorption in ZnF_2 Sample A Versus $T^{\frac{1}{2}}$

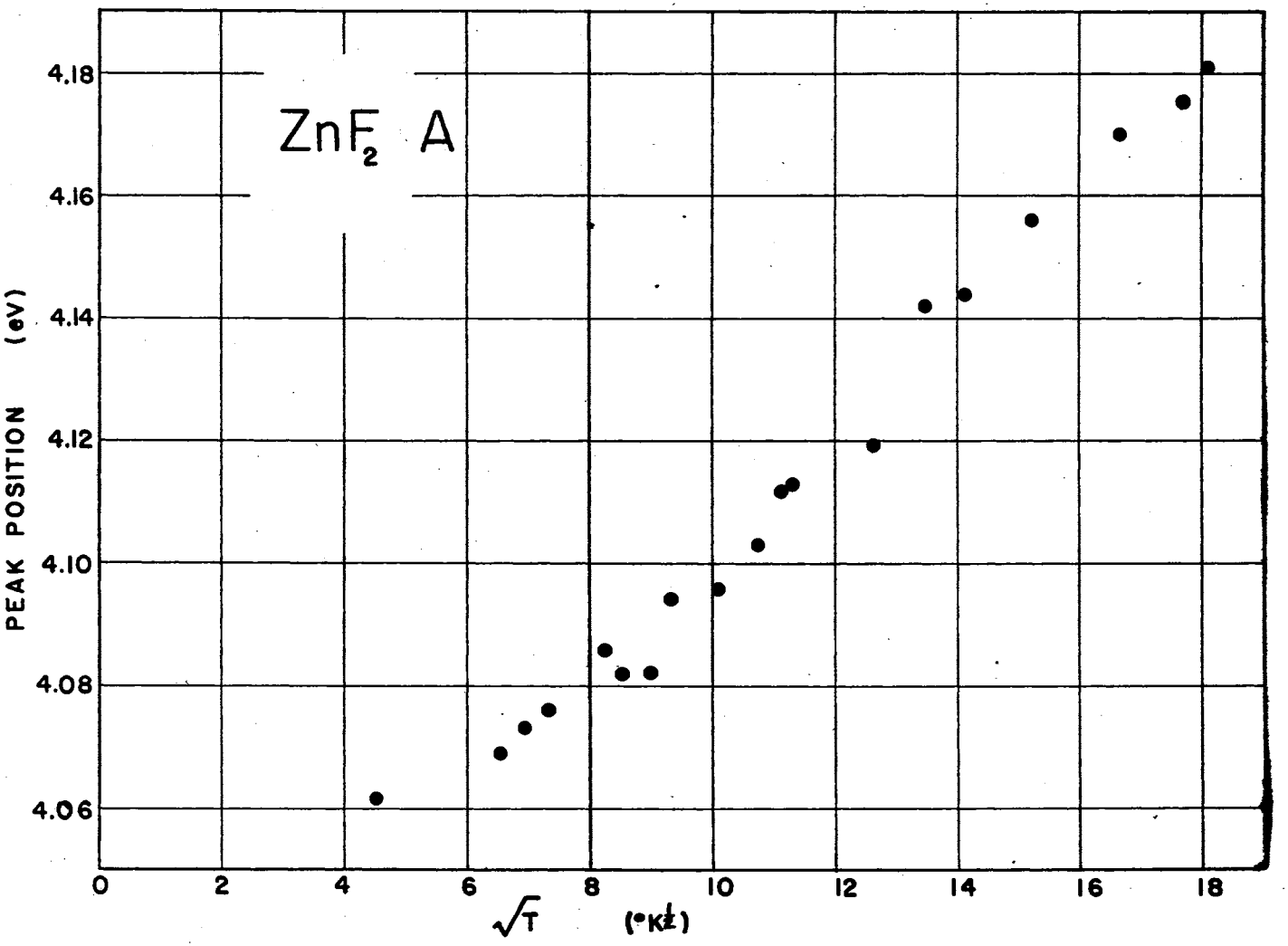

Figure 19. Peak Position of C_{2h} F_2 Absorption in ZnF_2 Sample A Versus $T^{\frac{1}{2}}$

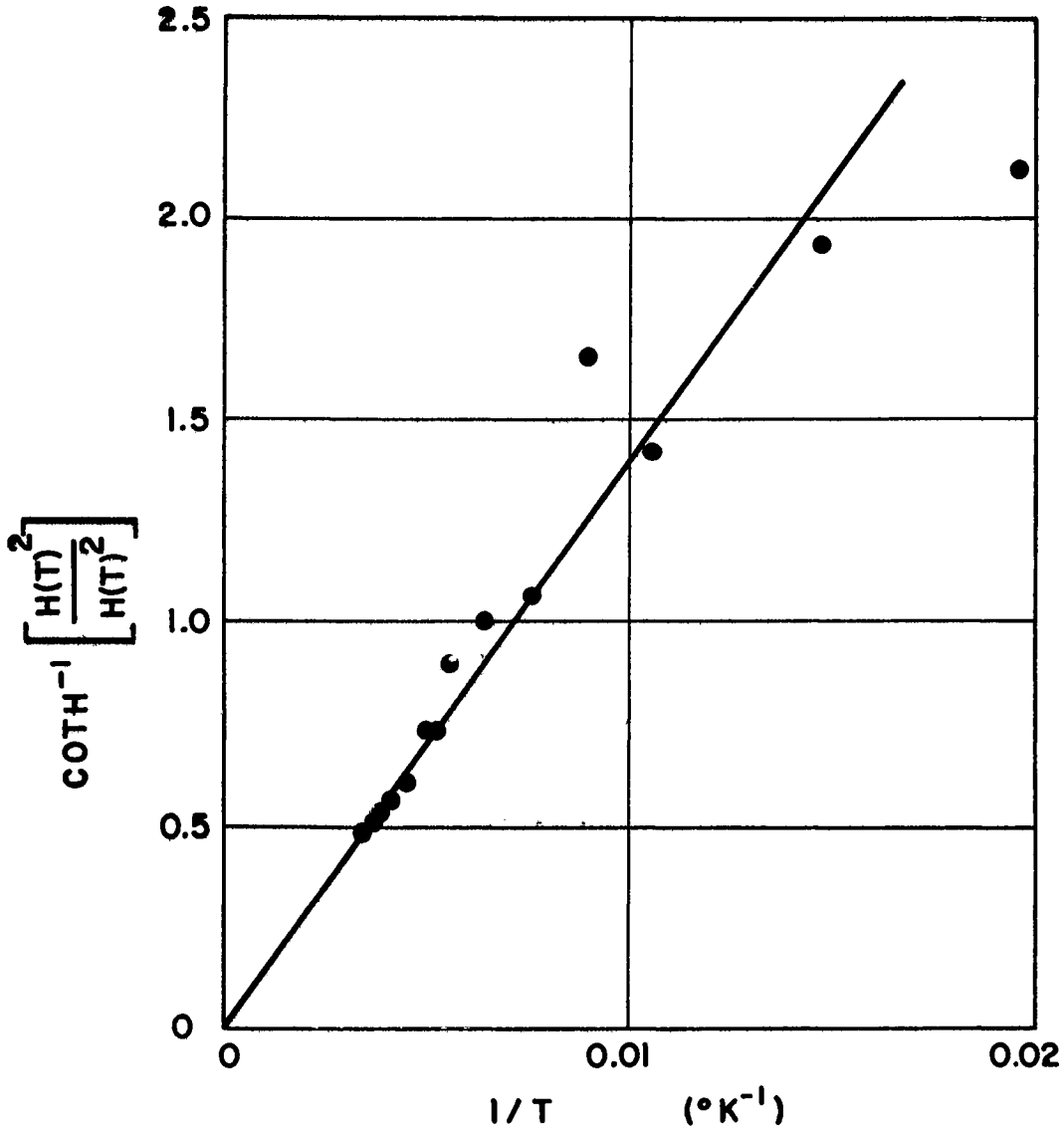

Figure 20. Arc Coth $[H(T)^2/H(0)^2]$ Versus 1/T for ZnF_2 Sample C

value found, approximately 53, is far above the maximum value at which one would expect to find a no-phonon absorption line associated with this center. A high resolution scan of the appropriate sample orientation and wavelength range was made for sample A at 4 K. No zero-phonon lines were found. From the relation developed earlier for the Stokes shift expected on this simple model, we would expect a luminescence associated with the σ transition of the C_{2h} center in ZnF_2 at about 1.55 eV (800 nm). Samples containing C_{2h} F_2 centers were excited at room temperature with 4.1 eV light, and the spectral region from 1.4 to 3.1 eV was searched. No luminescence bands were found. Excitation at 5.2 eV, in the F absorption, gave similarly negative results. It is quite possible that this luminescence is thermally quenched at room temperature. A luminescence band associated with this center in MgF_2 has been studied by Facey and Sibley[3,4]. It is very near the location predicted for it on the basis of the simple configuration coordinate model utilized by them.

We discussed in Chapter III the similarity of the F center to the classic particle in a box. This is the basis for the well-known Mollwo-Ivey relation between the peak positions of the F absorption bands and the lattice constant[30,31,38]. The peak position of the F band in the various alkali halides is rather well predicted by this relation[1], and even the transitions of the F_2 centers in these materials are found to follow a similar law[1,57]. Because the F centers in any material are somewhat like those in the alkali halides, it might be expected that these centers in many crystals would follow a similar relation. The peak positions of the F, C_{2h} F_2, and C_1 F_2 centers at room temperature are, respectively, 4.8, 3.4, and 3.1 eV in MgF_2, and 5.2, 4.1, and 3.5

eV in ZnF_2. Zinc fluoride has the larger lattice constants[69] (a = 4.703, c = 3.134 A for ZnF_2; a = 4.623 and c = 3.052 A for MgF_2), but its principal color-center bands lie uniformly at higher energies--a result not predicted by the Mollwo-Ivey relation. The answer to this contradiction lies most likely in the effects of ion size and consequent lattice effects discussed by Wood[38] and by Hays and Stoneham[70]. (Reference to Figure 1 may be helpful in what follows.) The normally accepted radii of Mg^{2+}, Zn^{2+} and F^- are, in order, 0.65, 0.74, and 1.36 A[71]. The (110) diagonal distance across the unit cell on a (100) face in MgF_2 is 6.66 A for ZnF_2 and 6.54 A for MgF_2. Adding the appropriate ionic diameters, one obtains a value for the space along this diagonal which the ions would take up if they were free to do so. For ZnF_2, this space is 6.92 A and for MgF_2, 6.74 A. The ions in ZnF_2 would take up 4% more space than is available, if they were free to do so, and those in MgF_2 only 3% more. Because of the steeply rising shape of the interatomic potential for small internuclear separations, this difference is significant. Thus, the F and F_2 centers in MgF_2 are already contained in smaller volumes than the simple Mollwo-Ivey relation assumes; those in ZnF_2 are even more restricted, in contrast to the expectation based solely upon a comparison of their lattice constants.

This crowding of the ions in the lattice may explain the lack of the expected biaxial polarization pattern for the C_{2h} F_2 center in c_1 crystals of ZnF_2. Study of a three-dimensional model of this lattice reveals that relaxation of the remaining lattice ions into the vacancies forming the center may force this center to reorient into one of several energetically equivalent but orientationally inequivalent directions. As a result of such reorientation, the expected biaxial pattern simply

would not exist. Biaxial symmetry is not found in similarly cut crystals of MgF_2, either. Another observation which may also be understood from these considerations is the shift toward lower energies of the peak position of the C_{2h} F_2 absorption with decreasing temperature. On the simple Mollwo-Ivey model, one would expect the absorption energies of a band to move toward higher energies as the lattice contracted. Again, reference to Figure 1 reveals that, for this particular center, the inter-vacancy distance, which affects the energy of the σ transition, could easily increase as the lattice ions contracted around it. That is, as the lattice atoms moved closer together, the vacancies would be forced to reorient and separate slightly, lowering the energy of the σ transition. There is no reason to expect that the π transition of this center or the F transition would be affected in this way. These latter two transitions, which are basically similar in nature, should depend directly on the volume available to each vacancy. The σ transition of the C_{2h} center should be relatively insensitive to this quantity. Reference to Table I of Chapter IV indicates that the 5.2 eV F absorption indeed moves toward higher energies with decreasing temperatures. Evidence that the same behavior exists for the π transition of the C_{2h} F_2 center in ZnF_2 is presented below.

The π Transition of the C_{2h} F_2 Center in MgF_2

The MgF_2 crystal employed in this work was a $c_{\parallel}$ specimen originally obtained from the Harshaw Chemical Company. It was used for the work described in references 65 and 66, and had been irradiated at room temperature with 2 MeV electrons to an unspecified dose. The only absorptions detectable at room temperature in the as received crystal were a

large F band at about 4.7 eV and a very small C_{2h} F_2 band near 3.4 eV. To obtain the π transition of the latter center, the crystal was bleached in steps at room temperature using the same procedures and equipment described earlier. After each bleach, the $\varepsilon \| c$ and $\varepsilon \perp c$ optical absorption spectra were measured. Under such treatment, the F absorption decreases very little in successive bleaches, while the F_2 band increases markedly. By subtracting the spectrum of the unbleached sample from the $\varepsilon \| c$ spectra obtained after successive bleaches, a difference curve was obtained which showed those bands which grew or diminished greatly as a result of bleaching. This difference spectrum is shown in Figure 21. The curves labeled 2-5 are the difference spectra taken after the 2nd, 3rd, ... bleaches. It can be seen that a band with peak position near 267 nm (4.64 eV) grows in as the sample is bleached. The slight depression at shorter wavelengths arises from that part of the decrease of the F band not compensated by growth of the 4.64 eV band. When this effect is taken into account, the actual peak of the 4.64 eV band is found to be closer to 4.70 eV. Figure 22 shows the relation between growth of the 4.7 eV absorption in the $\varepsilon \| c$ spectrum with the corresponding growth of the σ transition of the C_{2h} F_2 center at 3.4 eV in the $\varepsilon \perp c$ spectrum. It is a linear relation with a slope of approximately 0.72. Thus, it is reasonable to conclude that the band at 4.7 eV belongs to the π transition of the C_{2h} F_2 center. The relative oscillator strengths for the two transitions should be given by the ratios of the areas of the two absorptions. According to Smakula's equation, introduced in Chapter IV, this ratio should in turn be equal to the ratio of the products of peak height and half width for each band. Presence of the small F contribution in Figure 22 makes it difficult to obtain an accurate value for the

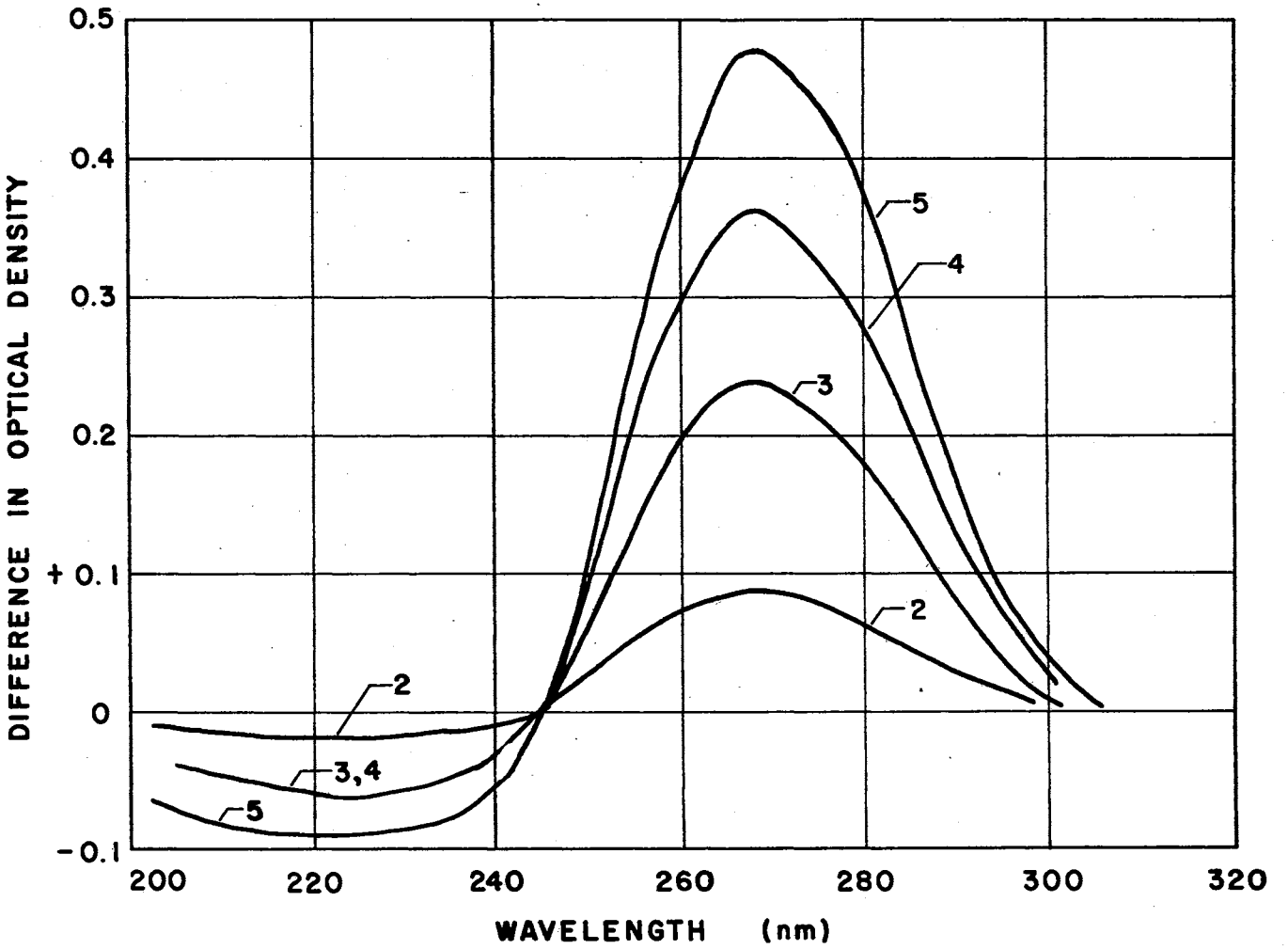

Figure 21. Difference Curve of $\varepsilon \| c$ Spectra Taken After Successive Bleaches Showing the π Transition of the C_{2h} F_2 Center Under the F Band in ZnF_2

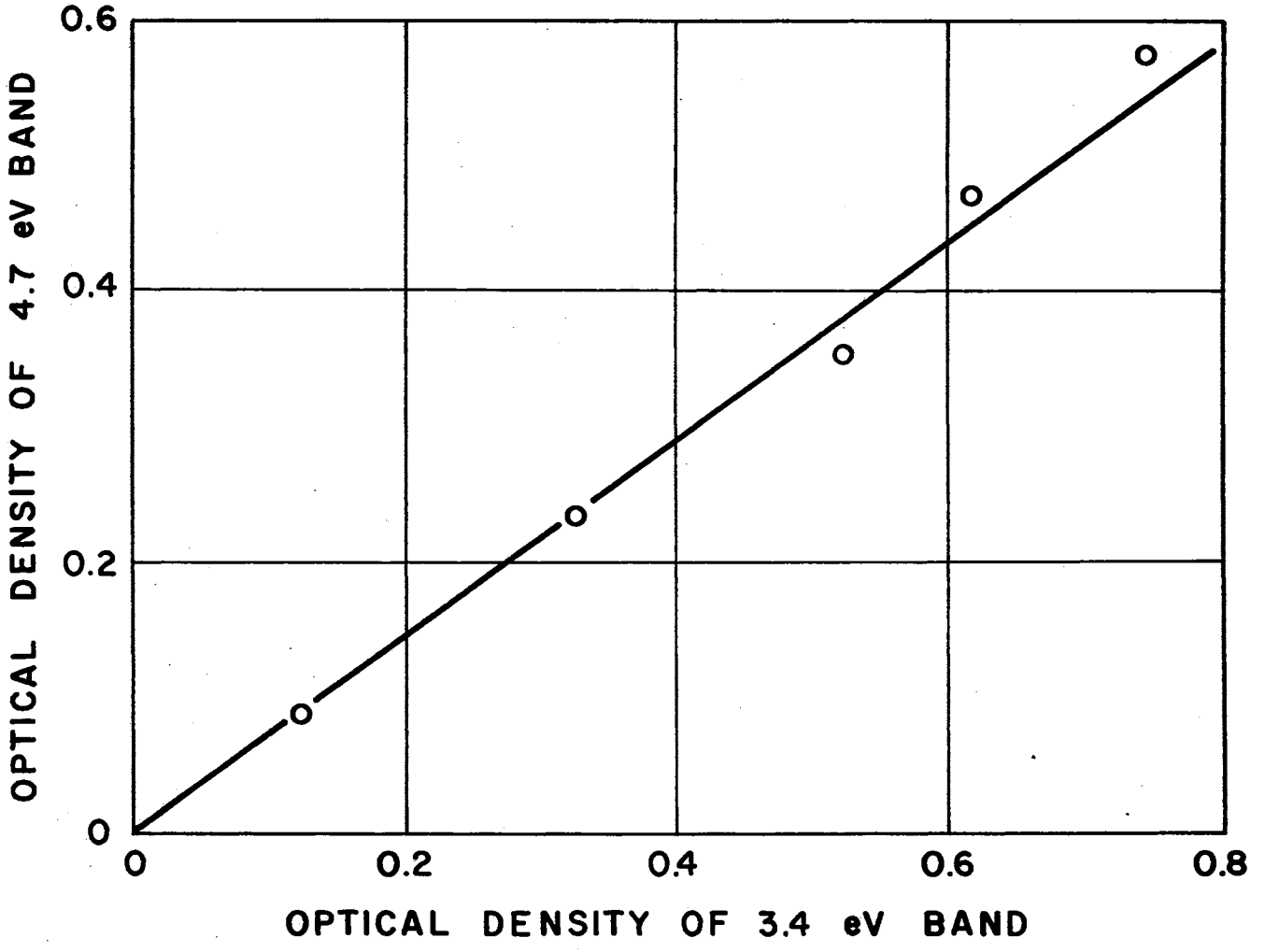

Figure 22. Relationship of the Height of the 4.70 eV Band to that of the 3.4 Band in ZnF_2

half width of the 4.7 eV band. Taking a value of 0.6 eV for this quantity, and the value of 0.24 eV measured by Facey and Sibley for the 3.4 eV band, the oscillator strength for the π transition is found to be approximately twice that of the σ. This does not arise from the fact that there are two energetically degenerate π transitions for the F_2 center. The light used to obtain $\varepsilon \| c$ spectra only samples one of these transitions, due to the geometry of the centers in the lattice. This can be seen with the aid of Figure 1. Moreover, examination of this figure leads one to expect that the two π transitions probably are not energetically degenerate, and occur at different energies in these materials just as in alkali halides.

Identification of the absorption at 4.7 eV is made even more positive by the data shown in Figure 23. The figure presents the excitation spectrum of the 2.95 eV luminescence associated with the σ transition of the C_{2h} F_2 center[65]. To obtain this spectrum, the intensity of the 2.95 eV emission was monitored while the exciting source was swept over the range 2-6 eV. The spectrum presented has been corrected for the variation of the intensity of the exciting source with energy. No self-absorption corrections were necessary because the exciting light was incident on the front face of the sample. Both the expected peak at the energy of the σ transition and one other peaking at 4.73 eV are found. This latter peak is undoubtedly the absorption found above at 4.70 eV. Presence of this higher-energy peak in the excitation spectrum for the luminescence associated with the σ-polarized absorption indicates that there is considerable mixing of the wavefunctions for the two excited states. The mixing may not be quite as great as could be inferred from the figure, however, for the absorption oscillator strength of the 4.7

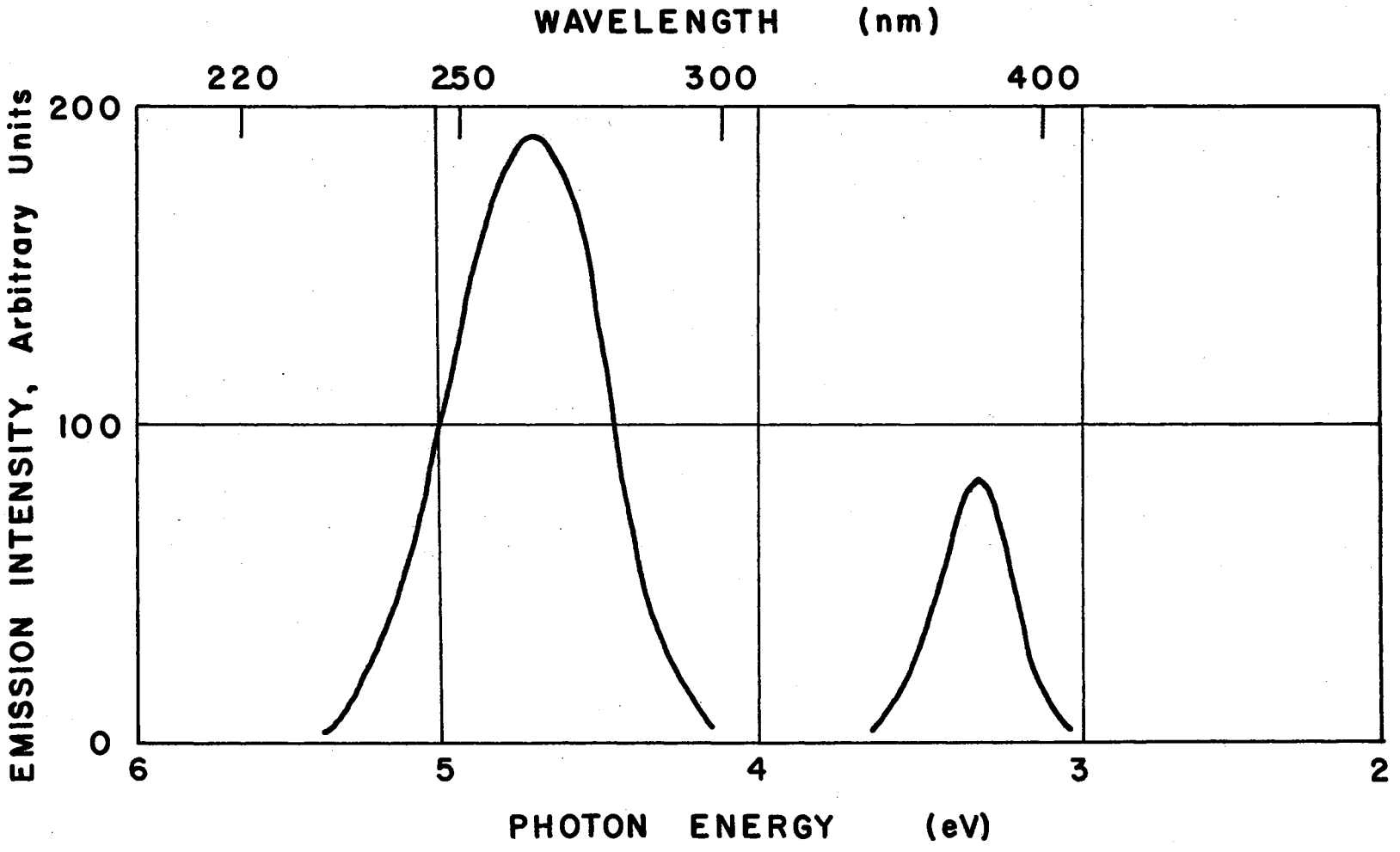

Figure 23. Excitation Spectrum of the 2.95 eV Luminescence in MgF_2

eV peak is larger than that of the other by a factor of two, and both π transitions were possibly excited in this measurement. Even with these corrections, about half of the energy absorbed by the π transition appears as emission from the σ transition.

Other Transitions of F_2 Centers

As the optical bleaching treatment just described for MgF_2 was continued past spectrum 5, the last one included in Figure 21, the D_{2h} F_2 center at 4.2 eV began to become significant in the $\varepsilon \| c$ absorption spectrum. This made the subtractions to obtain the height of the 4.7 eV absorption difficult. This same effect, however, allowed a determination of the approximate position of the π transition for the D_{2h} F_2 center in MgF_2. Figure 24 shows two second difference curves. The solid curve was obtained by subtracting difference curve 5 of Figure 21 from one which was the difference between spectra obtained after bleaches 9 and 6: the dotted curve is a similar reduction obtained by subtracting curve 3 of Figure 21 from the difference curve of bleaches 8 and 5. This plot, then, yields an indication of any absorptions appearing in the later stages of bleaching which were not present in earlier stages. It is apparent that there is an absorption peaking about 5.1 eV. Association of this absorption with that of the π transition of the D_{2h} center is made only as a plausible suggestion, because the second difference curves were not of sufficient accuracy to allow a correlation plot for this band similar to that shown in Figure 22 for the C_{2h} center.

When ZnF_2 sample C, a $c_\perp$ specimen, was bleached to obtain C_{2h} F_2 centers for the temperature dependence studies reported above, a new band which had not been noticed in $c_\parallel$ specimens was observed near 4.7

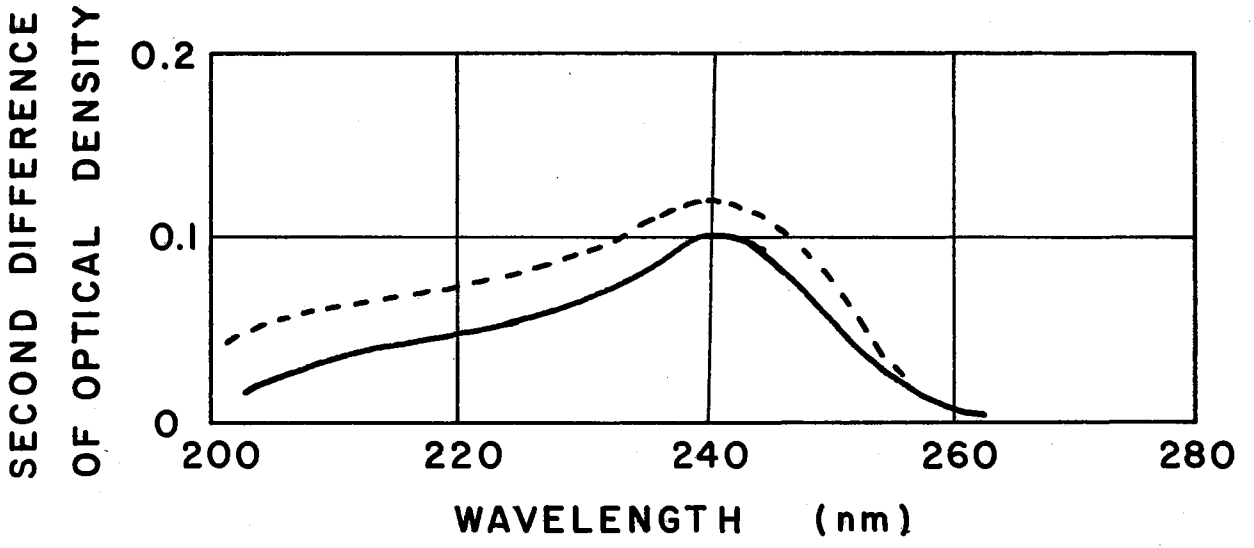

Figure 24. Second Difference Curves of ε||c Spectra Taken After Successive Bleaches Showing the π Transition of the D_{2h} F_2 Center Under the F Band in ZnF_2

eV. This band is evident in Figure 15. A subsequent search for it in spectra taken on $c_{\parallel}$ specimens revealed that it was present only in $\varepsilon \parallel c$ spectra and not present in any spectrum not containing C_{2h} F_2 centers. Because of these facts, and because it occurs in the proper energy range, it is suggested that this band arises from the π transition of the C_{2h} F_2 center. At 80 K, the peak position of this band has shifted to 4.86 eV, and at 10 K, it falls at 4.96 eV.

CHAPTER VI

SUMMARY AND SUGGESTIONS FOR FURTHER WORK

Summary

A Bridgman crystal growth apparatus capable of achieving temperatures high enough to grow any of the alkaline earth fluorides has been constructed. It has been used to grow ZnF_2 single crystals from which optical quality specimens were cut for the experiments described in this work.

The absorption spectra resulting from bombardment of ZnF_2 by 2 MeV electrons has been measured for irradiation temperatures from 15 to 370 K. The major bands resulting from such treatment peak near 3.5, 5.2 and 6.1 eV. Growth characteristics and region of thermal stability of the 3.5 eV band are those which often are associated with the $[F_2^-]$ center--a hole self trapped on two adjacent anions. The 5.2 and 6.1 eV absorptions were found to have similar growth characteristics at the temperatures used. The 5.2 eV absorption was tentatively identified as arising from the F center, but no serious changes would have to be made in any interpretations given if future research proves this assignment to be incorrect. This material was found to damage by a photolytic process; knock-on type damage was shown to play a minor role. Detailed damage mechanisms in MgF_2 were discussed, using a model recently proposed by Pooley which explains the observed features of the F center growth curves at temperatures between 4 and 300 K. It was concluded that the model

proposed for MgF_2, while useful for ZnF_2 cannot explain the observed growth characteristics of the 5.2 or 6.1 eV bands in the temperature range between 15 and 150 K. Two modifications of the MgF_2 process which could account for the observed behavior were discussed. One model in which the probability of a lattice anion reaching an interstice is temperature dependent, was suggested as the simpler and more physically probable.

When irradiated MgF_2 is bleached with light having an energy in its F-band region, a set of new color centers is generated which have previously been positively identified as belonging to one of several F_2 type centers. When certain irradiated crystals of ZnF_2 were similarly treated, a set of absorption bands appeared which had a direct correspondence to those found in MgF_2. These bands in ZnF_2 were tentatively identified by analogy with those having similar symmetries and peak energies in MgF_2. The σ and π transitions of the C_{2h} F_2 center in ZnF_2 were found to fall at 4.1 and 4.7 eV, respectively. From the variation of the half width of the σ transition, the effective frequency of the lattice mode most strongly coupled to this center was measured as approximately 5.8×10^{12} Hz at zero K. The full width at half maximum was found to be 0.41 eV. The Huang-Rhys factor computed from these values was 53--too high for an observable zero-phonon line. The peak position of this band was found to vary anomalously with temperature. A possible explanation for this phenomenon, utilizing the fact that the ions in the ZnF_2 lattice are relatively crowded, was offered. The π transition of the MgF_2 C_{2h} F_2 center was obtained by an analysis of polarized absorption data. The energy of the π transition was measured as 4.70 eV at 300 K. An excitation spectrum taken using the known luminescence band

from this center verified the assignment of the absorption band found.

Suggestions for Further Work

Although the band appearing under electron bombardment at low temperatures was suggested to be the $[F_2^-]$ center, it is imperative that a positive identification be made for two reasons. First, no similar absorption has been found for MgF_2 irradiated at any temperature. To discover which ones of the possible forms for this center in the rutile lattice actually exist is of interest in its own right. This center is of primary importance in the radiolysis process, however, and ZnF_2 shows marked differences in its damage characteristics from MgF_2 in the region around the temperature where this center apparently becomes unstable. It seems even more important, then, that the identity of the 3.5 eV band be investigated before more detailed work is done on the radiation damage processes in ZnF_2.

In the same vein, it seems wise, perhaps using ENDOR or Faraday rotation measurements, to positively identify the absorption arising from the F center in ZnF_2 before attempting to further elucidate the damage mechanism in this material. Because one inherently expects very close F center/interstitial pairs to occur in this lattice, it also seems necessary to establish the identity of the 6.1 eV band--or of whichever of the pair of bands at 5.2 and 6.1 eV is not the F center. If this band proved to be the perturbed F center, then the origin of the observed broadening of the 5.2 eV band in ZnF_2 and of the F band in MgF_2 would have to be carefully investigated. A search should be made for the corresponding high energy band in MgF_2 at photon energies beyond those employed so far.

The radiation damage process in these two materials is an intriguing problem, and should be investigated in some detail. As a next step after identification of the optical absorption bands, the damage at temperatures above about 500 K should be examined. If the suggestion made by Pooley for the damage mechanism in MgF_2 has applicability to ZnF_2, the damage rate should again increase in this temperature regime. If it did not, then at the very least, a modified form of the MgF_2 high temperature damage process would have to be sought.

While attempting to produce F_2 centers in ZnF_2 samples by bleaching, it was found that none could be made in the crystals grown at this institution. Only in the Bureau of Standards ZnF_2 crystals could such centers be produced. These latter crystals were known to contain perhaps 200 μg/g Mn, but nothing was known about their impurity content otherwise. Starting material of the highest available purity was used for the locally grown crystals. For this reason, it is possible that the centers actually made in the crystals studied were of the F_{2A} or F_{2Z} type rather than isolated F_2 centers. If this is so, the F_{2A} or F_{2Z} centers in these crystals exhibit the same polarization properties as isolated F_2 centers. If, on the other hand, the centers studied were indeed of pure F_2 type, then one must explain why they could not be produced in what are assumed to be considerably purer crystals. From such studies in alkali halides, ideas of the stabilities and mobilities of color centers not possessing optical absorptions have been gained. A similar benefit could be reaped from careful bleaching experiments in these ZnF_2 crystals. Concurrent with these studies, a search for the D_{2h} F_2 center in ZnF_2 and for higher-aggregate centers in both ZnF_2 and MgF_2 should be made.

A search was made for the luminescence band associated with the C_{2h} F_2 σ transition in ZnF_2. None was found at room temperature. A beginning configuration-coordinate diagram for this center could be established if the energy of this luminescence could be determined and its width measured as a function of temperature. Therefore, a search for this emission should be conducted at lower temperatures.

BIBLIOGRAPHY

1. Schulman, J. H. and W. D. Compton, Color Centers in Solids, The MacMillan Company, New York, 1962.

2. Turner, T. J., N. N. Isenhower, and P. K. Tse, Solid State Comm. 7, 1661 (1969).

3. Van Doorn, C. Z., Rev. Sci. Instr. 32, 755 (1961).

4. Vehse, W. E., O. E. Facey, and W. A. Sibley, Phys. Stat. Sol. 1, 679 (1970).

5. Datz, S., C. Erginsoy, G. Leibfried, and H. O. Lutz, Annual Reviews of Nuclear Science 17, 129 (1967).

6. Farge, Y., M. Lambert, and A. Gunier, J. Phys. Chem. Solids 27, 499 (1966).

7. Billington, D. S. and J. H. Crawford, Jr., Radiation Damage in Solids, Princeton University Press, Princeton, N. J., 1961.

8. Holmes, D. K., in Interaction of Radiation With Solids, R. Strumane, J. Nihoul, R. Gevers, and S. Amelinckx, eds., North Holland Publishing Co., Amsterdam, 1964.

9. Crawford, J. H., Jr., Adv. in Phys. 17, 93 (1968).

10. Sonder, E. and W. A. Sibley, in Defects in Solids, J. H. Crawford, Jr., and L. M. Slifkin, eds., Pergammon Press, Oxford, 1972.

11. Hersh, H. N., Phys. Rev. 148, 928 (1966).

12. Konitzer, J. D. and H. N. Hersh, J. Phys. Chem. Solids 27, 771 (1966).

13. Pooley, D., and W. A. Runciman, Solid State Comm. 4, 351 (1966).

14. Jette, A. N., T. L. Gilbert, and T. P. Das, Phys. Rev. 184, 884 (1969).

15. Pooley, D., Proc. Phys. Soc. 87, 257 (1966).

16. Still, P. B. and D. Pooley, Phys. Stat. Sol. 32K, 147 (1969).

17. Sibley, W. A. and O. E. Facey, Phys. Review 174, 1076 (1968).

18. Compton, W. D. and H. Rabin, Solid State Physics 16, 121 (1964).

19. Bridgman, P. W., Proc. Am. Acad. Arts Sci. 60, 303 (1925).

20. Stockbarger, D. C., Rev. Sci. Instr. 7, 133 (1936).

21. Stockbarger, D. C., Discussions Faraday Soc. 5, 294, 299 (1949).

22. Laudise, R. A., The Growth of Single Crystals, Prentice-Hall, Inc., Englewood Cliffs, N. J., 1970.

23. Brice, J. C., The Growth of Crystals From the Melt, North Holland Publ. Co., Amsterdam, 1965.

24. Tiller, W. A., The Art and Science of Growing Crystals, J. J. Gilman ed., Wiley, New York, 1963, pp. 277 ff.

25. Chandreskar, S., Hydrodynamic and Hydromagnetic Stability, Clarendon Press, Oxford, 1961.

26. Wilcox, W. R. and Fullmer, L. D., J. Appl. Phys. 36, 2201 (1965).

27. Brice, J. C., J. Crystal Growth 2, 395 (1968).

28. Hurle, D. T. J., in Crystal Growth, H. S. Peiser ed., Pergammon Press, Oxford, 1967, pp. 659 ff.

29. Fowler, W. B., in Physics of Color Centers, W. B. Fowler, ed., Academic Press, New York, 1968, p. 54.

30. Mollwo, E., Nachr. Ges. Wissen. Göttingen 97, (1931).

31. Ivey, H., Phys. Rev. 72, 341 (1947).

32. Gourary, B. S. and F. J. Adrian, Phys. Rev. 105, 1180 (1957).

33. Gourary, B. S. and F. J. Adrian, Solid State Physics 10, 127 (1960).

34. Laughlin, C., Solid State Commun. 3, 55 (1965).

35. Kojima, T., J. Phys. Soc. Japan 12, 918 (1957).

36. Wood, R. F., Phys. Rev. Letters 11, 202 (1963).

37. Wood, R. F. and H. W. Joy, Phys. Rev. 136, A451 (1964).

38. Wood, R. F., J. Phys. Chem. Solids 26, 615 (1965).

39. Born, M., and J. R. Oppenheimer, Ann. Physik 84, 457 (1927).

40. Dexter, D. L., Solid State Physics 6, 353 (1958).

41. Fowler, W. B. and D. L. Dexter, Phys. Rev. 128, 2154 (1962).

42. Fowler, W. B. and D. L. Dexter, J. Chem. Phys. 43, 768 (1965).

43. Markham, J. J., F-Centers in Alkali Halides, Academic Press, New York (1966).

44. Klick, C. C., D. A. Patterson and R. S. Knox, Phys. Rev. 133, A1717 (1963).

45. Klick, C. C. and J. H. Schulman, Solid State Physics 5, (1957).

46. Williams, F. E., J. Chem. Phys. 19, 457 (1951).

47. Williams, F. E., Phys. Rev. 82, 281 (1951).

48. Williams, F. E. and M. H. Hebb, Phys. Rev. 84, 1181 (1951).

49. Keil, T. H., Phys. Rev. 140, A601 (1965).

50. Fitchen, D. B., in Physics of Color Centers, W. B. Fowler, ed., Academic Press, New York, 1968, p. 293.

51. Gilbert, R. L. and R. F. Wood, J. Luminescence 1, 610 (1970).

52. Mostoller, M., B. N. Ganguly, and R. F. Wood, Phys. Rev. B4, 2015 (1971).

53. Henry, C. H. and C. P. Slicter, in Physics of Color Centers, W. B. Fowler, ed., Academic Press, New York, 1968, p. 351.

54. Mostoller, M., et. al., Phys. Rev. B4, 2667 (1971).

55. Herman, R., M. C. Wallis and R. F. Wallis, Phys. Rev. 10, 87 (1956).

56. Evarestov, R. A., Opt. Spectry (USSR) 16, 198 (1964).

57. Meyer, A., and R. F. Wood, Phys. Rev. 133, A1436 (1964).

58. Buckton, M. R., and D. Pooley, private communication, 1972; submitted for publication in J. Phys. C.

59. Ritz, V. H. and C. H. Cheek, Radiation Res. 25, 537 (1965).

60. Oen, O. S., ORNL Report 3813, May (1965).

61. Smakula, A., Z. Physik 59, 603 (1930).

62. Dexter, D. L., Phys. Rev. 101, 48 (1956).

63. Fermi, E., Nuclear Physics; Notes by J. Orear, et. al. The University of Chicago Press, Chicago, Ill., 1950, p. 32.

64. Sibley, W. A. and J. R. Russell, J. Appl. Phys. 36, 810 (1965).

65. Facey, O. E. and W. A. Sibley, Phys. Rev. 186, 926 (1969).

66. Facey, O. E. and W. A. Sibley, Phys. Rev. B2, 1111 (1970).

67. Stair, R., W. E. Schneider and J. K. Jackson, Appl. Opt. 2, 1151 (1963).

68. Blunt, R. F. and M. I. Cohen, Phys. Rev. 153, 1031 (1967).

69. Stout, J. W. and S. A. Reed, J. Am. Chem. Soc. 76, 5279 (1954).

70. Hays, W. and A. M. Stoneham, Phys. Letters 29A, 519 (1969).

71. Greenwood, N. N., Ionic Crystals, Lattice Defects and Nonstoichiometry, Butterworths, London, 1968.

VITA

Charles Thomas Butler

Candidate for the Degree of

Doctor of Philosophy

Thesis: RADIATION DAMAGE AND COLOR CENTERS IN ZnF_2 AND MgF_2

Major Field: Physics

Biographical:

Personal Data: Born in Muskogee, Oklahoma, November 30, 1932, the son of James and Vivian Butler.

Education: Attended primary and secondary schools in Joplin, Missouri; graduated from Joplin Senior High School in 1950; received Associate in Science degree from Missouri Southern College, Joplin, Missouri, in June 1952; received Bachelor of Science from Iowa State University with major in physics in December, 1954; received Master of Science degree in physics from Texas A and M University, College Station, Texas, in June, 1957; attended the University of Tennessee, Knoxville, Tennessee, part-time, 1960-1966; attended Oklahoma State University, Stillwater, Oklahoma, 1970-1972; completed requirements for the Doctor of Philosophy degree in July, 1972.

Experience: Employed as Research Assistant in the Physics Department of Iowa State University, Ames, Iowa (1953-1954) and as Graduate Teaching Assistant (1955); Graduate Teaching Fellow in Physics Department of the Texas A & M University, College Station, Texas (1955-1956); Research Scientist at the Caltech Jet Propulsion Laboratory, Pasadena, California (1956-1960); Research Physicist in the Solid State Division of the Oak Ridge National Laboratory, Oak Ridge, Tennessee (1960-1970); Instructor in the Physics Department of the Oklahoma State University, Stillwater, Oklahoma (1970-1972).

Organizations: Member of the Society of Sigma Xi, American Physical Society and American Association for Crystal Growth.